OPTIMAL DIMENSIONLESS DESIGN AND ANALYSIS OF JET EJECTORS AS COMPRESSORS AND THRUST AUGMENTERS

A Thesis

by

GANESH MOHAN

Submitted to the Office of Graduate Studies of
Texas A&M University
in partial fulfillment of the requirements for the degree of

MASTER OF SCIENCE

May 2006

Major Subject: Mechanical Engineering

OPTIMAL DIMENSIONLESS DESIGN AND ANALYSIS OF JET EJECTORS AS COMPRESSORS AND THRUST AUGMENTERS

A Thesis

by

GANESH MOHAN

Submitted to the Office of Graduate Studies of
Texas A&M University
in partial fulfillment of the requirements for the degree of

MASTER OF SCIENCE

Approved by:

Co-Chairs of Committee,	Othon K. Rediniotis
	Luis San Andres
Committee Member,	Malcolm Andrews
Head of Department,	Dennis O' Neal

May 2006

Major Subject: Mechanical Engineering

ABSTRACT

Optimal Dimensionless Design and Analysis of Jet Ejectors as Compressors and Thrust Augmenters. (May 2006)

Ganesh Mohan, B.Tech, Indian Institute of Technology Madras, India

Co-Chairs of Advisory Committee: Dr. Othon K. Rediniotis
Dr. Luis San Andres

A jet ejector may be used as a compressor or to enhance thrust of watercraft or aircraft. Optimization of jet ejectors as compressors and thrust augmenters was conducted using the software GAMBIT (Computer Aided Engineering (CAE) tool for geometry and mesh generation) and FLUENT (Computational Fluid Dynamics (CFD) solver kit). Scripting languages PYTHON and SCHEME were used to automate this process.

The CFD model employed 2D axis symmetric, steady-state flow using the $k-\varepsilon$ method (including wall functions) to model turbulence. Initially, non-dimensionalization of the jet ejector as a gas compressor was performed with respect to scale, fluid, and operating pressure. Surprisingly, rather than the conventional parameters like Mach or Re number, the results showed a completely new parameter (christened GM - Gauge Mach) that when kept constant will result in non-dimensionalization.

Non-dimensionalization of a jet ejector for watercraft propulsion was conducted using 2D axis symmetric, steady-state flow modeling using the $k-\varepsilon$ method (including wall functions). It showed consistent results for the same velocity ratio (r) of nozzle velocity to free-stream velocity for different scales, fluids, and ambient pressures.

Optimization studies showed that there is an increase in thrust of ~5% when $r \approx 10$. The increase is more for larger r values. Beyond $r \approx 15$, where the percentage increase in thrust reaches 15%, there is not much appreciable change in thrust. At $r \approx 65$, the thrust enhancement peaks at ~25%, but this large r is not practical.

DEDICATION

I dedicate this thesis to amma (mom), appa (dad) and akka (sister) – Mrs. Kala Mohan, Mr. V. Mohan and Radhika Mohan for their unconditional love and unflinching support for all my gargantuan ambitions in life.

ACKNOWLEDGEMENTS

I am grateful to my advisor, Dr. Othon K. Rediniotis, for his constant support and encouragement to manage two to three research projects simultaneously. His carefree style makes any problem look simple and easy.

I would like to thank Dr. Luis San Andres and Dr. Malcolm Andrews for being very patient and understanding of my problems. Their support was necessary for every step I took to achieve my master's degree.

Words cannot express my gratitude to Dr. Mark T. Holtzapple for his unending guidance and support throughout this project. Without his innovative ideas, this project would not have been possible.

Special thanks to my best friends – Dipa Brahmbhatt, Kaushik Balakrishnan, Manoj Gupta, Preethi, Seeja and Bharath for being with me in all my good and bad times together.

I would like to thank Somsak Watanavanavet for being a great teammate in the times when we were working together for this project. Thanks to Manoranjan Majji for being an understanding teammate in our times together for "The Morphing Wing" project.

TABLE OF CONTENTS

Page

Page

LIST OF FIGURES

FIGURE Page

FIGURE Page

FIGURE Page

LIST OF TABLES

NOMENCLATURE

C_p	Non-dimensional pressure at any non-dimensional location on the jet ejector (dimensionless)
P_s	Static pressure at any non-dimensional location on the jet ejector (Pa)
P_o	Static pressure at outlet of jet ejector (Pa)
ρ_p	Average density of propelled flow at inlet (kg/m^3)
v_p	Average velocity of propelled flow at inlet (m/s)
X	Non-dimensional *x*-axis (dimensionless)
x	Real *x*-axis (m)
L	Length of jet ejector (m)
GM_m	*GM* for motive flow at nozzle of jet ejector (atm)
P_{ms}	Static pressure of motive flow at nozzle (Pa)
M_m	Mach number of motive flow at nozzle (dimensionless)
GM_p	*GM* for propelled flow at inlet of jet ejector (atm)
P_{ps}	Static pressure for propelled flow at inlet (Pa)
M_p	Mach number of propelled flow at inlet (dimensionless)
D_p	Diameter of propelled flow (m)
D_n	Diameter of nozzle of the jet ejector (m)
D_t	Diameter of the throat of jet ejector (m)

D_o Diameter of the outlet of the jet ejector (m)

X_t Position of the throat and nozzle of the jet ejector (m)

M_n Momentum of nozzle (N)

V_n Velocity of nozzle (m/s)

ρ Density of fluid (kg/m^3)

A_n Area of cross section of nozzle = $\pi D_n^2 / 4$ (m^2)

P_n Static pressure of nozzle (Pa)

F_{net} Net force acting on a free body diagram (N)

F_{wo} Net force acting on the outer wall of the nozzle in the direction of thrust (N)

F_{wi} Net force acting on the inner wall of the nozzle in the direction of thrust (N)

F_w Total force acting on the outer wall of the nozzle in positive x-direction (N)

T^1 Thrust of the nozzle jet without the ejector shroud (N)

T Thrust of the nozzle jet with the ejector shroud around it (N)

T_n Net thrust acting on the walls of the ejector shroud (N)

T_s Total thrust from the surfaces of Jet ejector (inner-outer walls, nozzle wall) (N)

C_D Coefficient of drag for the outer surface of the nozzle ~ 0.04 for a smooth surface (dimensionless)

P_{st} Static pressure at any given location in the flow domain (Pa)

P_∞ Ambient pressure for the flow domain (Pa)

P Power of the nozzle jet (W)

$\dot{m}$	Mass flow rate of nozzle jet (kg/s)
v	Velocity of nozzle jet (m/s)
A_p	Area of the propeller equivalent to cross-sectional area of nozzle (m^2)

INTRODUCTION

General

A jet ejector is a fluid dynamic pump. It pumps a low-energy secondary fluid using the kinetic energy of the primary stream. The pumping is done with no moving parts. Jet ejectors have been used in the past century as pumps, compressors, or thrust enhancers. Although this technology is old, it is still being pursued with the latest advanced tools to improve its performance, of which the most powerful tool is CFD. With more and more powerful supercomputers available at relatively economical costs, universities can afford them allowing researchers to perform numerical experiments (as they are popularly known) at a significant savings of energy, time, and cost compared to physical experiments. Many thousands of research papers (journals and conferences) have been published in the past two decades using CFD to substitute for the cost of inefficient wind-tunnel experiments. Lately, popular CFD softwares like FLUENT, CFX, and STAR-CD have simplified research by replacing the lengthy numerical codes for performing robust numerical experiments on a computer screen.

Although jet ejectors have been applied as thrust enhancers, they have mostly been restricted to aircrafts and rockets. They have not been used as thrust boosters for watercraft, like cargo ships, oil tankers, submarines, boats, jet skis or powered surf boards.

This thesis follows the style of ASME Journal of Energy Resources Technology.

Any breakthrough made in this field would replace conventional, low-efficiency propulsion systems. Hence, with this motive, we decided to take up this challenge. And, because water-tunnel experiments are expensive and time consuming, we pursued a complete CFD analysis to find the optimal design that would serve this purpose.

Because dimensionless analysis is the most powerful technique to reduce duplication or repetition of efforts to find the optimal design, we perform the analysis for jet ejectors used as both compressors and thrust augmenters. For compressors, the flow was compressible gas, whereas for thrust augmenters, it was incompressible liquid water. Here we were more interested in the optimal design for augmenting thrusts for watercraft. The compressor design was emphasized by Somsak Watanavanavet [1]. The dimensionless analysis of compressors reported here can be used by future researchers to speed optimization processes for obtaining maximum efficiency.

Literature survey

Jet ejectors can potentially be used as thrust augmenters in an aerodynamic lifting body to create external characteristics that greatly augment aerodynamic lift [2-3]. Ejectors have been used on aircraft engines to increase the thrust of a primary propulsive nozzle, but also to mix the high-temperature exhaust flow with ambient air to provide lower jet noise and plume radiation [4, 5].

Later researchers identified many possible ways to improve the thrust and pumping efficiency. For example, Walter et al. used forced mixer lobes in jet ejector designs [6].

With advances in science and technology, many new areas were identified for their application. Jet ejectors have been used in air-conditioning systems [7], absorption systems [8], and also as a heat sink for high-power dissipation electronics [9].

Although there have been design optimization studies of jet ejectors for rocket-based systems or compressors [10], there is almost no literature report that shows the use of CFD package like FLUENT to completely explore all possible shapes of jet ejectors to find the optimal shape that would give maximum thrust for watercraft, like cargo ships, submarines, oil tankers, jet skis, or powered surfboards.

Unfortunately, there is no literature available for the application of jet ejectors as thrust boosters for watercraft. This drives us to make a fresh beginning in this field, which has remained untapped so far. With no background research materials available, we started by performing numerical experiments. We decided to non-dimensionalize and find an optimal shape that enhances thrust. Then, we compared the results with conventional propulsion systems available for watercraft.

JET EJECTOR AS A COMPRESSOR

General

This section discusses the details of the design, case setup, and procedures of jet ejector used as a compressor.

Design

A jet ejector, as described in the introductory section, consists of a nozzle placed at the center (usually near the throat) of the ejector shroud. Our jet ejector is shown in Figure 1, Appendix A.

Figure 1, Appendix A, shows how a jet ejector can be used as a compressor. Here, the fluid (air) is propelled through the inlet diameter or propelled diameter (D_p) with the dragging force exerted by fluid (air) coming out of the nozzle of diameter D_n placed at the center of the throat of diameter D_t. Through this process, the fluid is compressed and exits through outlet diameter D_o.

Case setup and procedure

CFD analysis of a jet ejector as compressor can be performed using GAMBIT and FLUENT software with 2D axis symmetric, steady-state flow modeling using the $k-\varepsilon$ method (including wall functions) to model turbulence. Figure 2, Appendix A, shows

how the 2D axis symmetric design looks. For effective simulation in FLUENT, with pressure inlet/pressure outlet boundary conditions, the outlet diameter expands into an infinite volume (with diameter approximately 2 times the length of jet ejector).

DIMENSIONLESS ANALYSIS OF JET EJECTOR AS COMPRESSOR

General

This section discusses dimensionless analysis of a jet ejector used as a compressor. It shows the definition and analysis of various parameters used for the analysis, including a noble parameter which is newly christened as *GM* (Gauge Mach). Our objective is to find a parameter (e.g., Re, Mach) – which when kept constant irrespective of changes in scale (e.g., 1×, 1.5×, 2×), fluid (e.g., air, steam, nitrogen), and operating pressure (e.g., 0.1…1…10 atm) – will ensure the same non-dimensional pressure (C_p) at any non-dimensional location on the jet ejector. In this way, one can eliminate infinite numbers of cases and thereby save time and money, before getting into the actual optimization.

Definitions

1. Non-dimensional pressure

Non-dimensional pressure is defined as the increase in static pressure at any non-dimensional location on the jet ejector over the static pressure at the outlet, non-dimensionalized by the dynamic pressure at the propelled inlet.

$$C_p = \frac{P_s - P_o}{\frac{1}{2}\rho_p v_p^2} \tag{1}$$

2. Non-dimensional x-axis

The x-axis is non-dimensionalized with respect to the total length (L) of the jet ejector. Figure 3, Appendix A, gives a sketch of compressor design. Hence, the non-dimensionalized x-axis is defined as

$$X = \frac{x}{L} \tag{2}$$

3. Noble parameter, *GM*

GM – Newly christened as Gauge Mach, a noble parameter that works for our analysis

$$GM_m = P_{ms} M_m \tag{3}$$

Similarly,

$$GM_p = P_{ps} M_p \tag{4}$$

GM_m and GM_p are the parameters – if when kept constant irrespective of changes in scale, fluid, or operating pressure for a given geometrical shape of jet ejector – ensures the same non-dimensional pressure C_p at any non-dimensional location X.

Analysis

To arrive at a parameter that influences non-dimensional analysis, we need to play with the variables one at a time. Hence, we do the following.

1. Different scales of jet ejector with same Mach number

Table 1, Appendix B, shows data of cases having the same fluid (air) and operating pressure (1 atm), but with varying scales (1×, 1.5× and 2×) of the jet ejector for the same Mach number of both motive and propelled flow. Mach number is considered because these are compressible flows. For our convenience *Cp* is compared along the walls of the jet ejector. Figure 4, Appendix A, shows that for the same Mach number or *GM* value of both motive and propelled flow, non-dimensional pressure, *Cp* remains same irrespective of change in scale.

Table 2, Appendix B, and Figure 5, Appendix A, provide another example with a different Mach and *GM* values, but with similar conditions. Figure 5, Appendix A, once again proves that for the same Mach number or *GM* value of both motive and propelled flow, non-dimensional pressure *Cp* remains same irrespective of change in scale of jet ejector.

2. Different fluids with same Mach number

Table 3, Appendix B, shows changes in only the fluid (air, steam) while fixing the other parameters (scale =1×, operating pressure =1 atm) but with the same Mach number. Figure 6, Appendix A, proves that if the Mach or *GM* value is kept constant, *Cp* remains constant irrespective of change in fluid for a fixed scale and operating pressure.

Table 4, Appendix B, shows another example with different Mach and *GM* values, but with similar conditions as above. Figure 7, Appendix A, once again proves

that if Mach or *GM* value is kept constant, *Cp* remains constant irrespective of change in fluid for a fixed scale and operating pressure.

3. Different operating pressures with same Mach number

Table 5, Appendix B, shows the effect of different operating pressures if we keep the scale (1×), fluid (air), and Mach number the same. Note that the *GM* values for these cases are totally different from each other. Figure 8, Appendix A, indicates that for the same Mach number, *Cp* does not remain the same for different operating pressures with other parameters remaining same. We can also notice that *GM* values are also different for these cases. So, let us try with same *GM* values at motive and propelled, but for different operating pressures with everything else remaining the same.

4. Different operating pressures with same *GM* values

Table 6, Appendix B, shows results with different Mach numbers for different operating pressures. We find that the *GM* values once again remain the same. Figure 9, Appendix A, shows that when *GM* values are maintained constant, the *Cp* values also remain the same. The difference at the center of the plot can be attributed to the accuracy of the model (course mesh).

Let us consider another example and at different operating pressure ranges (Table 7, Appendix B). Here once again, we find that for the same *GM* value, Figure 10,

Appendix A, shows that the *Cp* remains the same irrespective of change in operating pressure.

5. Combination of all three (scale, fluid and operating pressure) for same *GM* values

Table 8, Appendix B, shows what happens if all three variations (fluid, scale, and operating pressure) are combined in one analysis with *GM* being constant for all at motive and propelled flow. Figure 11, Appendix A, again confirms that *GM* is the only valid parameter for non-dimensional analysis of jet ejectors. The small differences in Figure 11, Appendix A, are due to numerical error introduced by a coarse mesh.

Table 9, Appendix B, shows another example with the same *GM* value, but with all other parameters (scale, fluid and operating pressure) being different from the previous example. Figure 12, Appendix A, again confirms that when *GM* is kept constant, irrespective of other parameters, *Cp* remains the same.

Conclusion

For a given geometrical shape of jet ejector and for given values of *GM* for both propelled and motive flow, then the non-dimensional pressure (*Cp*) at any non-dimensional location on the jet ejector remains constant irrespective of scale, fluid, or operating pressure.

JET EJECTOR AS PROPELLERS

General

This section discusses the details of the design, case setup, and procedures of jet ejector used as a propeller.

Computational setup and procedure

Because jet ejectors are axis-symmetric in flow properties, 2D axis-symmetric flow modeling has been used. Figure 13, Appendix A, is a schematic of the 2D axis-symmetric jet ejector model used in our numerical experiments to find the optimum shape that maximizes efficiency.

The jet ejector was meshed in a huge rectangular box in the computational domain to perform the 2D axis-symmetric flow simulations using CFD software, FLUENT. The geometry meshed in GAMBIT is as shown in Figures 14 & 15, Appendix A.

The boundary conditions as given in FLUENT for this computational domain are as follows

1) Pressure inlet at domain inlet

2) Pressure outlet at domain outlet

3) Velocity inlet at the nozzle

With the given boundary conditions, an ambient static pressure of 101325 Pa is maintained in the computational domain for all the cases set for finding the optimum; hence, the static pressure at the nozzle obtained after the simulations will be relative to the ambient pressure.

It was found that convergence is attained soon after 1000 iterations for all cases solved using the $k-\in$ method having incompressible flow. It takes almost 2–3 hours of computational time in a supercomputer. The mesh was maintained fine with approximately 400,000 cells spanning the 2D domain.

Rapid creation of cases using journal files (PYTHON) in GAMBIT

GAMBIT was used to create the geometry and mesh it finely. The process is tedious if we have to do it for hundreds of geometries with different dimensions. Journal files overcome this tedium. A journal file records every step when creating and meshing geometry in GAMBIT. Hence, we can take advantage of this phenomenon by creating a clean journal file that only has those dimensions of the geometry to be entered in respective command lines. But, it cannot have a well-defined curve connecting those dimensions. We connect those nodes to be smooth and pleasant to the naked eye. But, we assume that the smoothness is not going to affect the optimized geometry. The difference is that we will get an optimized geometry that shows lower increase in thrust than possible. In the end, we can rectify that by introducing smoothness in the surface of optimized geometry obtained. For our reference, let us name the approximate shape that

we form connecting those nodes as the standard shape. The journal file in Appendix C was created for this purpose.

The journal file in Appendix C has comment lines with formulas that are numbered from 1 to 17 are to be calculated every time we create a new GAMBIT file; hence, there was a special Excel file created for this purpose. With this, the operational time drastically reduced when creating a case. There were about 5000 cases created for the optimization, of which only about 500 were useful. The journal file saved a great deal of time.

DIMENSIONLESS ANALYSIS AND OPTIMIZATION OF JET EJECTOR USED AS A PROPELLER

General

Non-dimensionalization is a very powerful tool for saving time. This section discusses definition, dimensionless analysis, and optimization of jet ejector as a propeller. Out of six dimensions that define the jet ejector, we set the length $L = 1$. This reduces the number to five. This can also be interpreted as non-dimensionalizing the dimensional variables with respect to L. This is done by dividing all other variables by $2L$ except X_t and L, which are divided by L.

These five non-dimensional variables are varied within physical limits in different combinations to determine the optimum geometry with the maximum increase in thrust.

Definition

The thrust of the nozzle jet without the ejector shroud (Figure 16, Appendix A), follows:

$$T^1 = M_n V_n - 0.5 C_D \rho A_n V_{fs}^2 \tag{5}$$

The thrust of the nozzle jet with the ejector shroud around it (Figure 17, Appendix A), follows:

$$T = M_n V_n + P_n A_n + T_s \tag{6}$$

The increased thrust from adding the shroud follows:

$$\text{Increase in thrust (\%)} = 100\frac{(T - T^1)}{T^1} \tag{7}$$

Derivation of thrust equations

The thrust acting on the nozzle without any ejector shroud around it (Figure 16, Appendix A) is equivalent to the net force acting on the nozzle.

$$F_{net} = F_{wo} + F_{wi} + M_n V_n \tag{8}$$

But,

F_{wo} = Pressure force + Drag force

$$= -P_n A_n - 0.5 C_D \rho A_n V_{fs}^2 \tag{9}$$

Also,

F_{wi} = Pressure force

$$= P_n A_n \tag{10}$$

Substituting Equations 9 and 10 into Equation 8 gives

$$F_{net} = M_n V_n - 0.5 C_D \rho A_n V_{fs}^2 \tag{11}$$

Or,

$$T^1 = F_{net} = M_n V_n - 0.5 C_D \rho A_n V_{fs}^2 \tag{12}$$

Figure 17, Appendix A, shows the free body diagram of nozzle with an ejector shroud around it. For this set up, the thrust force acting on the combination is derived as follows:

$$F_{net} = F_{wo} + F_{wi} + M_n V_n + T_n \tag{13}$$

But,

$$F_{wo} = -F_w \tag{14}$$

And,

$$F_{wi} = P_n A_n \tag{15}$$

Substituting Equations 14 and 15 into Equation 13 gives

$$F_{net} = M_n V_n + P_n A_n + (T_n - F_w) = M_n V_n + P_n A_n + T_s \tag{16}$$

Or,

$$T = F_{net} = M_n V_n + P_n A_n + T_s \tag{17}$$

Optimization

Optimization was done by running cases with many sensible combinations of dimensions of the jet ejector having different combinations of velocity ratio ($r = V_n / V_{fs}$). From Figures 21, 22 and 23, Appendix A, we find that for a given velocity ratio (r = 10) and other parameters remaining same, the percentage increase in thrust remains the same

irrespective of change in free stream velocity (V_{fs} = 6, 10 and 15 m/s). All the graphs indicate the plot of percentage increase in thrust vs. one non-dimensional parameter keeping other parameters as constants. These constants were chosen after various crude trial-and-error runs that indicated this combination to be approximately close to the optimum.

Figures 21 to 28, Appendix A, show the plots of percentage increase in thrust versus $D_t/2L$ and $D_o/2L$ keeping other parameters constant for all velocity ratios. There is a maximum increase in thrust for $D_o/2L$ = 0.1 and $D_t/2L$ = 0.12. To find the highest percentage increase in thrust, we vary $D_n/2L$ and X_t/L, keeping other parameters constant for a constant V_{fs} and $Re\,D_n$ (Reynolds number of nozzle). From Figure 29, Appendix A, we find that $D_n/2L$ = 0.01 gives the maximum increase in thrust. Figure 30, Appendix A, indicates that for X_t/L = 0.5 and for optimized $D_t/2L$ = 0.12, $D_o/2L$ = 0.1 and $D_n/2L$ = 0.01 keeping other parameters constant, the thrust increases its maximum percentage.

This observation drives us to the fact that $D_t/2L$ must be the mid-point of the straight line joining $D_p/2L$ = 0.15, and $D_o/2L$ = 0.1, because X_t/L = 0.5 is also the location of the throat. Hence, $D_t/2L$ = 0.125 instead of 0.12, because it is closer. So, after we redo the calculation for $D_t/2L$ = 0.125, Figure 31, Appendix A, confirms once again that $D_n/2L$ = 0.01 indicates the maximum increase in thrust. Also from Figure 32,

Appendix A, we observe that for $X_t/L = 0.5$ or having a straight line just connecting the propelled and outlet diameter of the shroud, there is a maximum increase in thrust. Hence, our assumption of $D_t/2L = 0.125$ is justified. So, the optimized geometry of the jet ejector (in our first series of iterations) that gives us the maximum increase in thrust for any combination of velocity of the vehicle and the Reynolds number of the nozzle is given in Table 10, Appendix B.

For the above dimensions, the internal shape of the shroud should be a straight line. But, the external shape can be changed to find the optimal one. We tried all 2D NACA profiles of airfoil like NACA 0012, 0015 (e.g., Figures 18 and 19, Appendix A). Of these, 0018, 0021 show the least drag for the same design parameters. We also tried a flat profile (e.g., Figure 20, Appendix A) forming both internal and external surfaces for the shroud. Table 11, Appendix B, compares all these for a free stream velocity of 2 m/s and nozzle velocity of 125 m/s (or $\mathrm{Re} = 2.49 \times 10^6$).

Hence, a simple flat profile for both internal and external surface of the shroud of the jet ejector gives the maximum increase in thrust. The optimized geometric profile is shown in Figure 20, Appendix A. This thrust increase of about 23.43% is the maximum possible for this combination of free-stream and nozzle velocities. In terms of velocity ratio, we find that $r = 62.5$ is the best, which is too high to be efficiently implemented in practice.

Hence, to find a range of optimized geometries that have achievable velocity ratios (r); we simulated a number of cases varying $D_n/2L$ and X_t/L with all other

parameters being constant. The percentage increases in thrust are shown in Figures 35 to 40, Appendix A. These plots indicate that for $r < 25$, the percentage increase in thrust reaches a maximum of only ~16%. Because, velocity ratios of $r > 2$ are the least efficient, the results are not that promising to have any practical significance. To finalize our conclusions, these results are compared with conventional engines in the last section.

The entire optimization was done assuming $D_p/2L = 0.15$ to be the exact optimized non-dimensional parameter. Table 12, Appendix B, shows the percentage increase in thrust for velocity ratio of $r = 15$ for $D_p/2L = 0.1$ and 0.2 in the range of other non-dimensional parameters that would verify our assumption.

Table 13, Appendix B, shows the combination of non-dimensional parameters for $r = 15$ and $D_p/2L$ that gives a maximum percentage increase of 10.13%, which is greater than the maximum percentage increases of 6.25% for $D_p/2L = 0.1$ and 9.26% for $D_p/2L = 0.2$. This verifies our assumption of $D_p/2L = 0.15$ is the best non-dimensional number around the optimum region.

Dimensionless analysis of optimized geometry of jet ejector

The most important entity in any dimensionless analysis is the non-dimensional pressure. Here it is defined as the increase in static pressure at any non-dimensional location on the jet ejector over the ambient pressure of the system, non-dimensionalized by the dynamic pressure of the free stream.

$$C_p = \frac{P_{st} - P_{\infty}}{0.5\rho V_{fs}^2} \tag{18}$$

This optimized geometry (Table 10, Appendix B) is non-dimensionalized such that for different scales, fluids, and ambient pressures, the non-dimensional pressure C_P at any given non-dimensional location remains the same.

From Figures 33 and 34, Appendix A, we find that the C_P plots match exactly for inner and outer surfaces of the jet ejector shroud. This proves that, irrespective of scale or fluid, or ambient pressure, the optimized geometry remains the same. Also the percentage increase in thrust remains the same for all of them (Tables 14 and 15, Appendix B).

DISCUSSIONS AND CONCLUSIONS

General

The optimized results are analyzed for their relevance in practical applications by comparing with a super tanker at one extent and a jet ski at the other.

Supertanker

Supertankers have an average propeller power of 20 MW (~28,000 SHP). Their average propeller diameter is about 6 m (~20 ft) and they cruise at average speeds of 7.5 m/s (~14.5 knots). Let us assume 100% efficiency for the nozzle. For these specifications, the following variables are calculated.

$$V_{fs} = 7.5\,\text{m/s}$$

$$A_p = \pi \frac{D_p^2}{4}$$

$$= \pi \frac{(6\text{m})^2}{4} = 28.274\ \text{m}^2$$

$$P = \frac{1}{2}\dot{m}v^2 = \frac{1}{2}\rho A_p v^3$$

$$v = \sqrt[3]{\frac{2P}{\rho A_p}} = \sqrt[3]{\frac{2(20\times10^6\ \frac{\text{kgm}^2}{\text{s}^3})}{(998.2\ \frac{\text{kg}}{\text{m}^3})(28.274\text{m}^2)}}$$

$$= 11.235\ \text{m/s}$$

Hence, if the propeller is replaced by a nozzle of same diameter then,

$$V_n = v = 11.235\ \text{m/s}$$

$$r = \frac{V_n}{V_{fs}} = \frac{11.235\text{m/s}}{7.5\text{m/s}} = 1.498 \cong 1.5$$

Because, the optimization results show decrease in thrust for r <= 5 (Figure 35, Appendix A), jet ejectors cannot be applied to watercraft like supertankers.

Now, to consider the other extreme scale in watercraft, a jet ski is the best bet.

Jet ski

Jet skis have an average power of 0.15 MW (~200 BHP). They have an average nozzle diameter of about 0.075 m (~3 inch) and they cruise at average speeds of 30 m/s (~65 mph). Let us again assume 100% efficiency for the nozzle. For these specifications, the following variables are calculated.

$$V_{fs} = 30\ \text{m/s}$$

$$A_p = \pi \frac{D_p^2}{4}$$

$$= \pi \frac{(0.075\text{m})^2}{4} = 0.004418\ \text{m}^2$$

$$P = \frac{1}{2}\dot{m}v^2 = \frac{1}{2}\rho A_p v^3$$

$$v = \sqrt[3]{\frac{2P}{\rho A_p}} = \sqrt[3]{\frac{2(0.15\times10^6\ \frac{\text{kgm}^2}{\text{s}^3})}{(998.2\frac{\text{kg}}{\text{m}^3})(0.004418\text{m}^2)}}$$

$$= 40.82\ \text{m/s}$$

Or,

$$V_n = v = 40.82\ \text{m/s}$$

$$r = \frac{V_n}{V_{fs}} = \frac{40.82\text{m/s}}{30\text{m/s}} = 1.36$$

Again, the velocity ratio *r* is much less than 5. Unfortunately, this indicates that jet ejectors cannot be applied to watercraft. The addition of an ejector shroud will reduce the thrust and thereby reduce the efficiency.

Conclusion

Jet ejectors are not the solution for improving thrusts in watercraft. The possibility is completely ruled out on the basis that jet ejectors provide an increase in thrust only beyond a velocity ratio *r* of 10 or more (Figures 36 to 40, Appendix A). But, because all watercraft ranging from high-speed jet skis to high-powered supertankers have velocity ratios less than 2. Adding jet ejectors would only reduce the thrust already attained, and thereby reduce the efficiency. Hence, our objective of finding thrust enhancement using jet ejectors unfortunately has given results that have no practical significance. Hence, it

can be concluded with our analysis that jet ejectors are not the solution for getting additional thrust enhancements for watercraft.

REFERENCES

1. Watanawanavet, S., 2005, "Optimization of a High-Efficiency Jet Ejector by Computational Fluid Dynamic Software", MS thesis, Texas A&M University, College Station, TX.

2. Quinn, B., 1970, "A Wind Tunnel Investigation of the Forces Acting on an Ejector in Flight," ARL 70-0141.

3. Whittley, D. C., 1967, "The Augmenter Wing Research Program Past Present and Future," AIAA Paper 67-741.

4. Kramer, J. J., Chestnutt, D., Krejsa, E. A., Lucas, G., and Rice, E. J., 1971, "Noise Reduction", Aircraft Propulsion, NASA SP-259, pp. 169-209.

5. Braden., R. P., Nagaraja, K. S., and von Ohain, H. J., 1982, "Ejector Workshop for Aerospace Application," AFWAL-TR-82-3059. AF-FDL.

6. Walter, M. Presz Jr., Morin, B. L., and Gousy, R. G., 1988, "Forced Mixer Lobes in Ejector Designs," Journal of Propulsion and Power, **4,** pp. 350-355.

7. Rogdakis, E. D., and Alexis, G. K., 2000, "Design and Parametric Investigation of an Ejector in an Air-Conditioning System," Applied Thermal Engineering, **20**(2), pp. 213-226.

8. Levy, A., Jelinek, M., and Borde, I., 2002, "Numerical Study on the Design Parameters of a Jet Ejector for Absorption Systems," Applied Energy, **72**(2), pp. 467-478.

9. Mahalingam, R., and Glezer, A., 2005, "Design and Thermal Characteristics of a Synthetic Jet Ejector Heat Sink," Journal of Electronic Packaging, **127**(2), pp. 172-177.

10. Jahingir, M. N., and Huque, Z., 2005, "Design Optimization of Rocket-Based Combined-Cycle Inlet/Ejector System," Journal of Propulsion and Power, **21**(4), pp. 650-655.

APPENDIX A

FIGURES

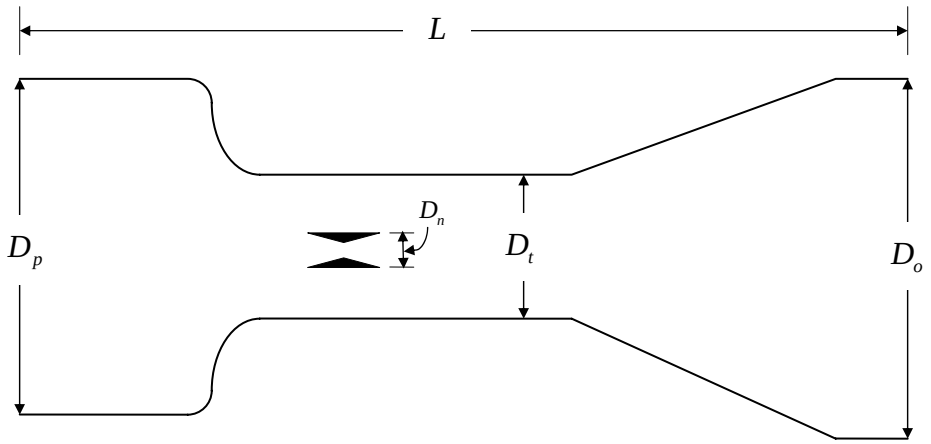

Figure 1: Sketch of jet ejector as a compressor.

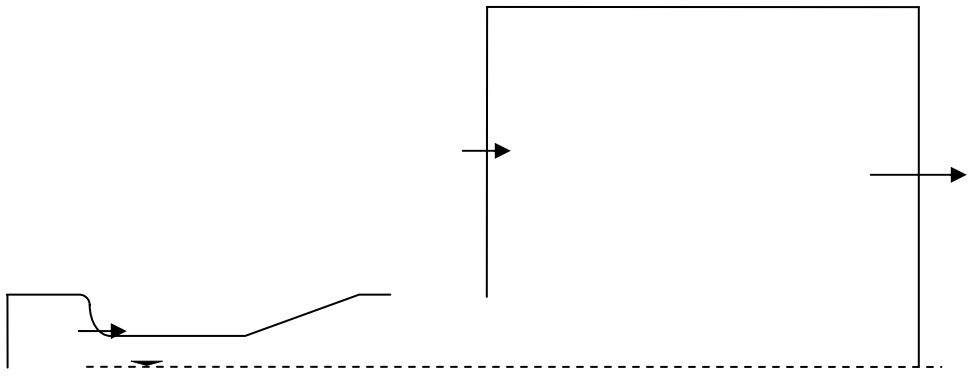

Figure 2: 2D axis symmetric mesh design of a compressor.

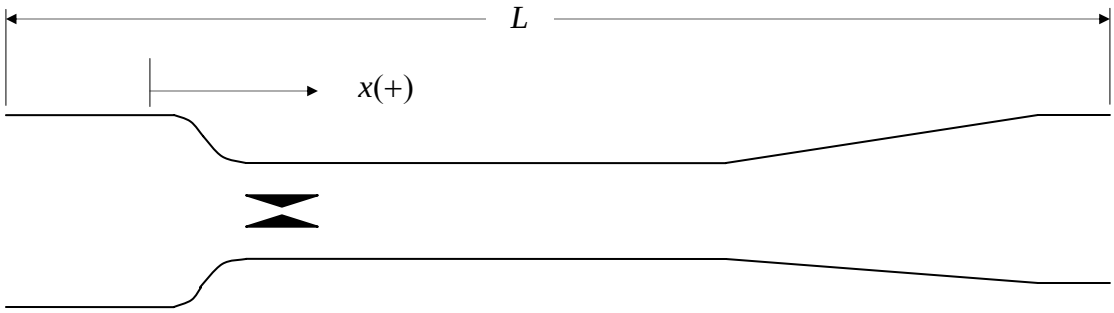

Figure 3: Sketch of the compressor design.

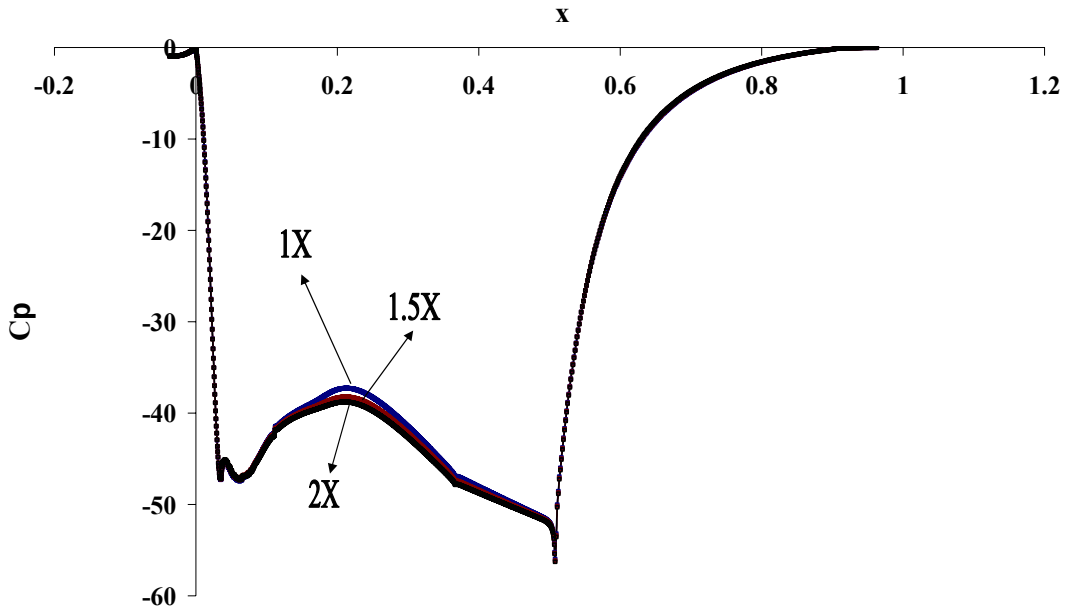

Figure 4: C_p along the walls of the jet ejector for cases discussed in Table 1, Appendix B.

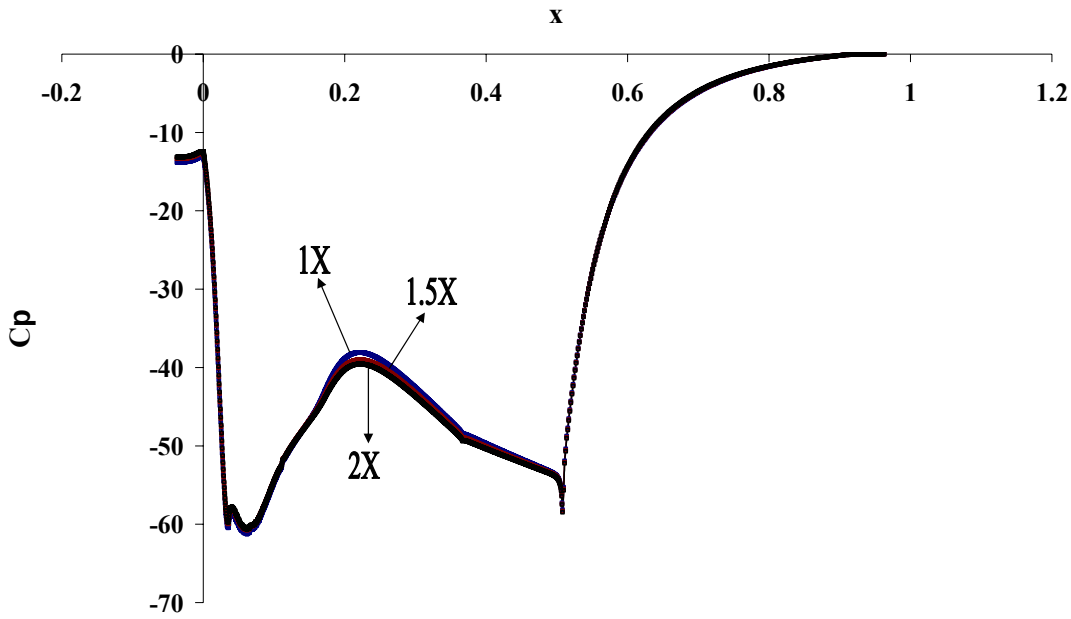

Figure 5: C_p along the walls of the jet ejector for cases discussed in Table 2, Appendix B.

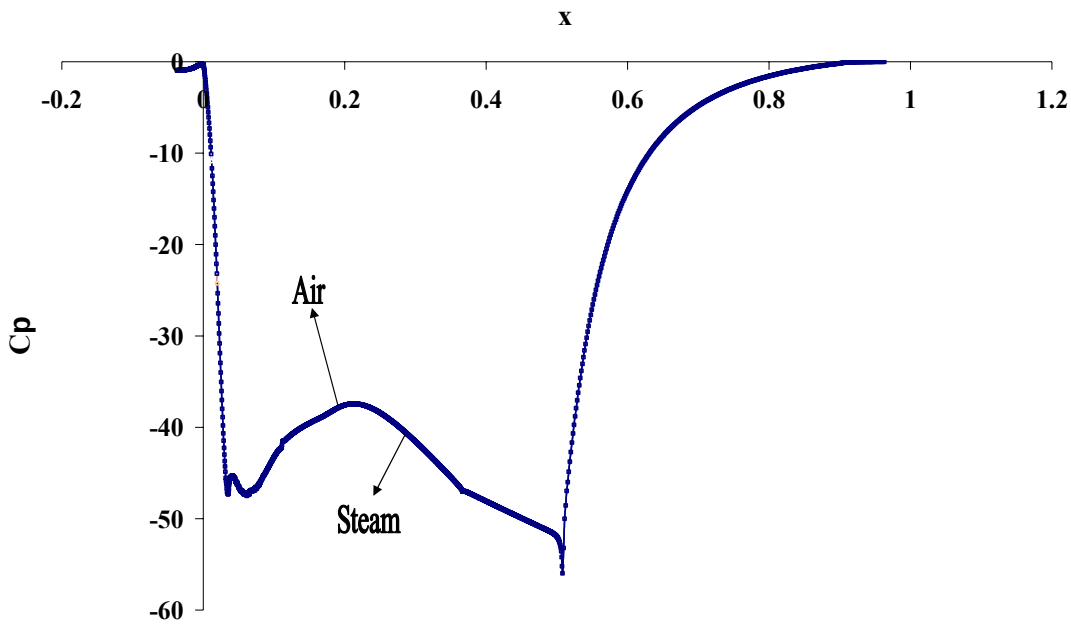

Figure 6: C_p along the walls of the jet ejector for cases discussed in Table 3, Appendix B.

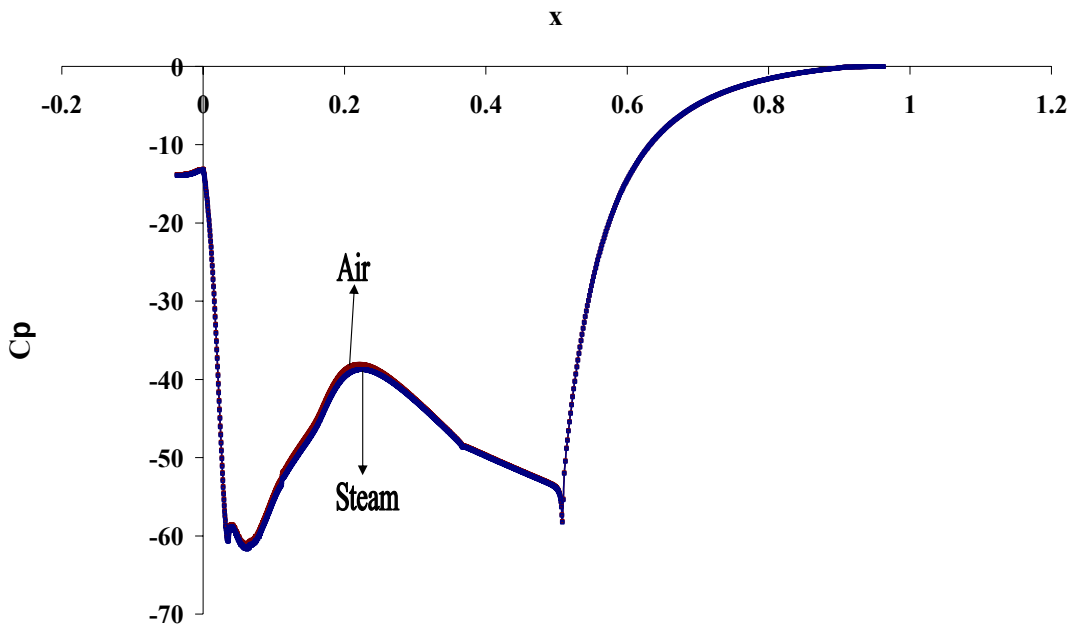

Figure 7: C_p along the walls of the jet ejector for cases discussed in Table 4, Appendix B.

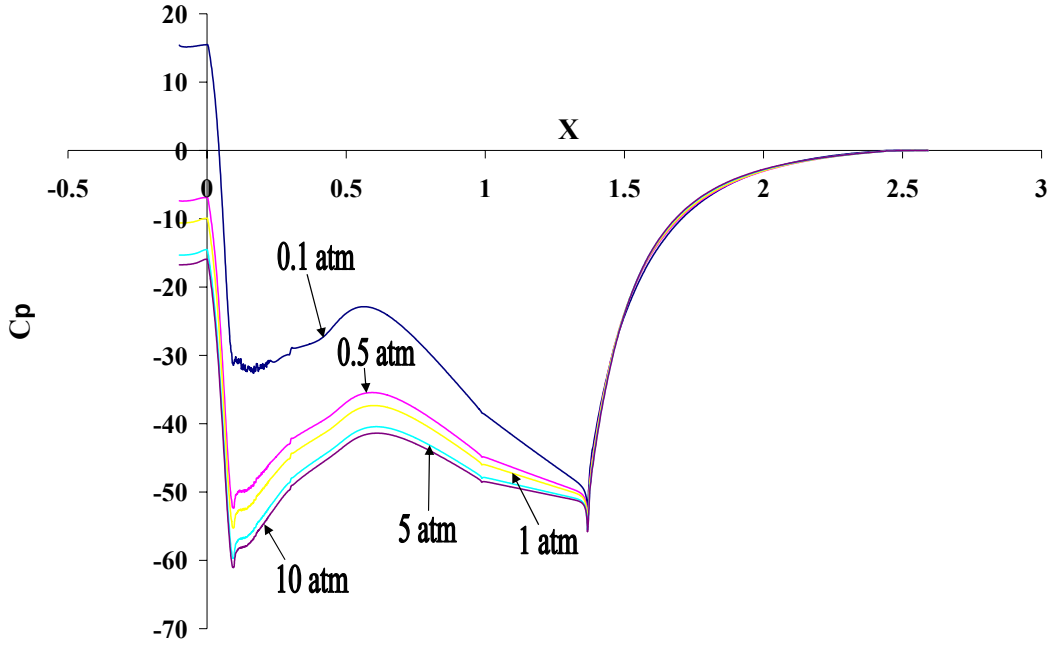

Figure 8: C_p along the walls of the jet ejector for cases discussed in Table 5, Appendix B.

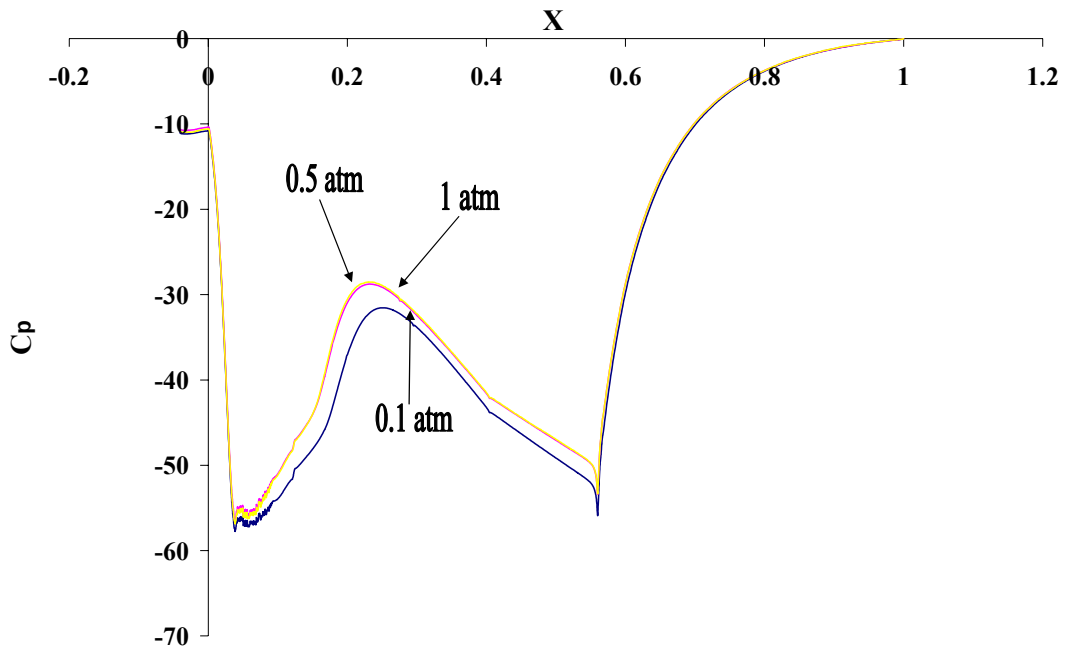

Figure 9: C_p along the walls of the jet ejector for cases discussed in Table 6, Appendix B.

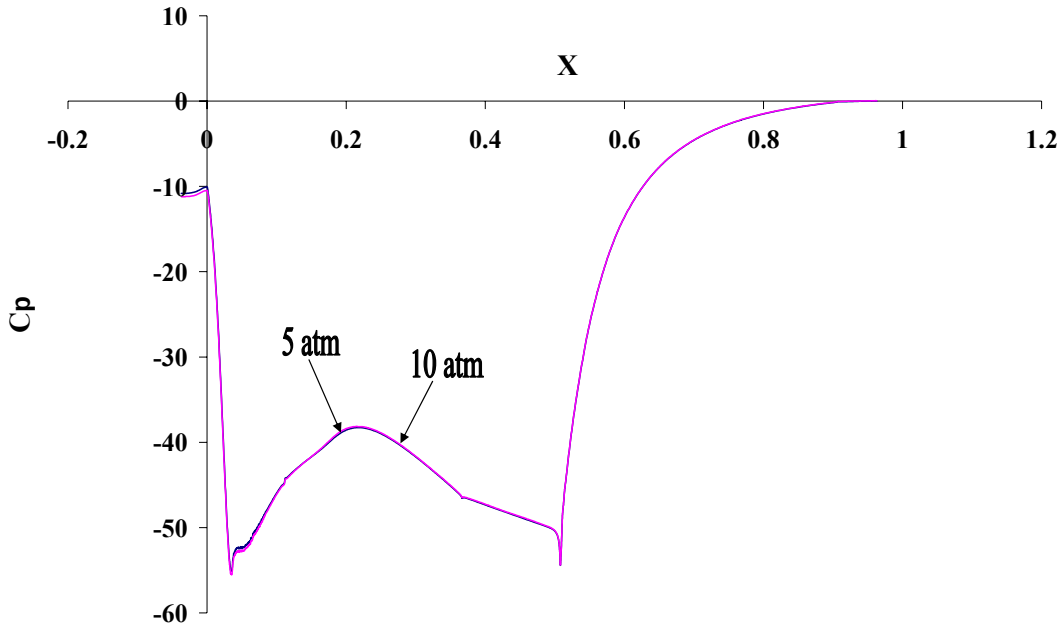

Figure 10: C_p **along the walls of the jet ejector for cases discussed in Table 7, Appendix B.**

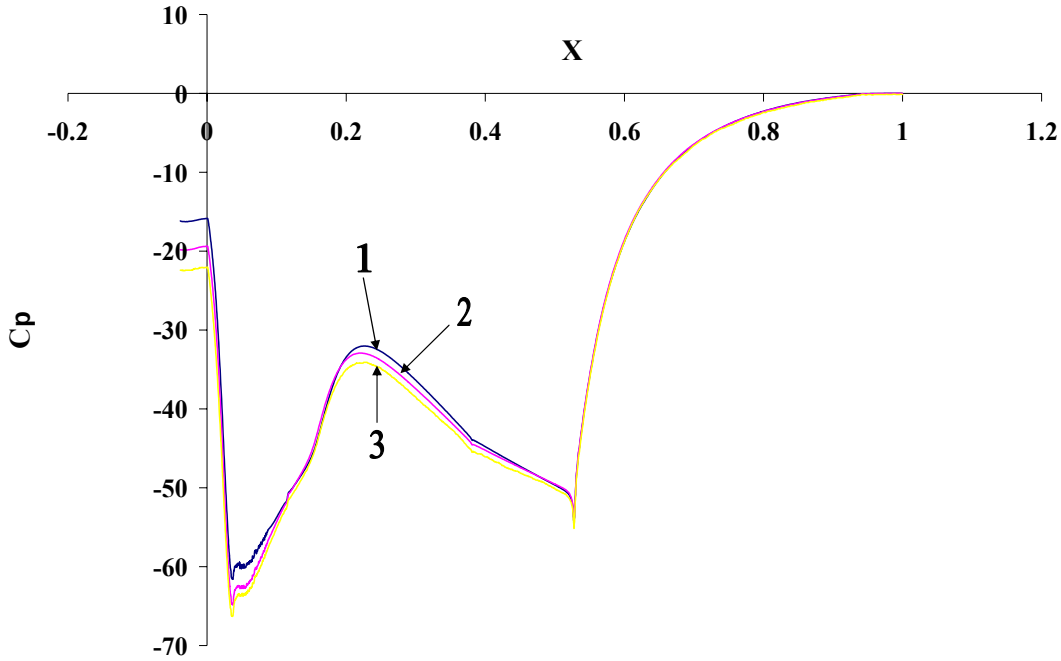

Figure 11: C_p along the walls of the jet ejector for cases discussed in Table 8, Appendix B.

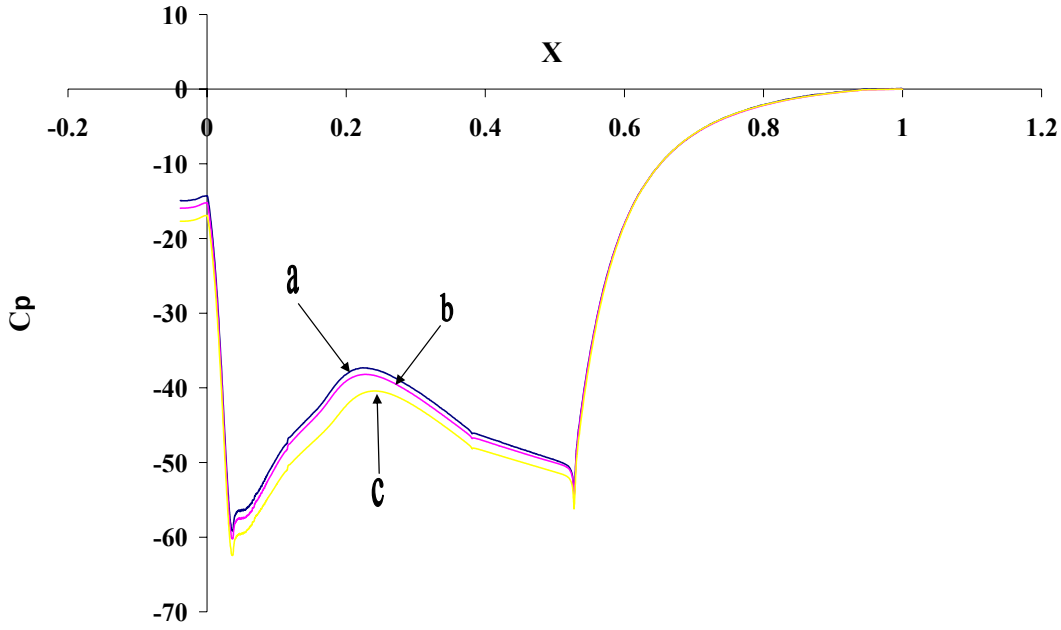

Figure 12: C_p along the walls of the jet ejector for cases discussed in Table 9, Appendix B.

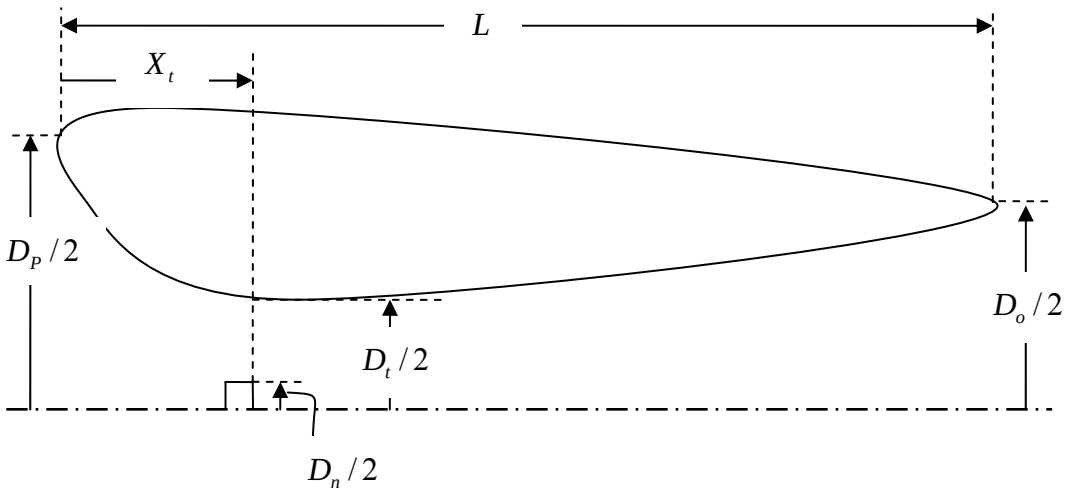

Figure 13: Jet ejector – axis symmetric model.

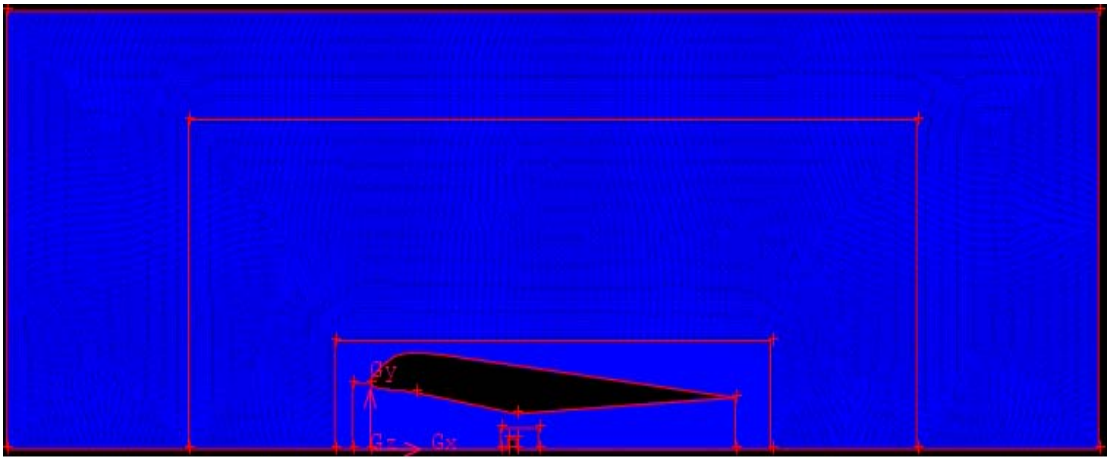

Figure 14: Jet ejector geometry meshed with rectangular domain in GAMBIT.

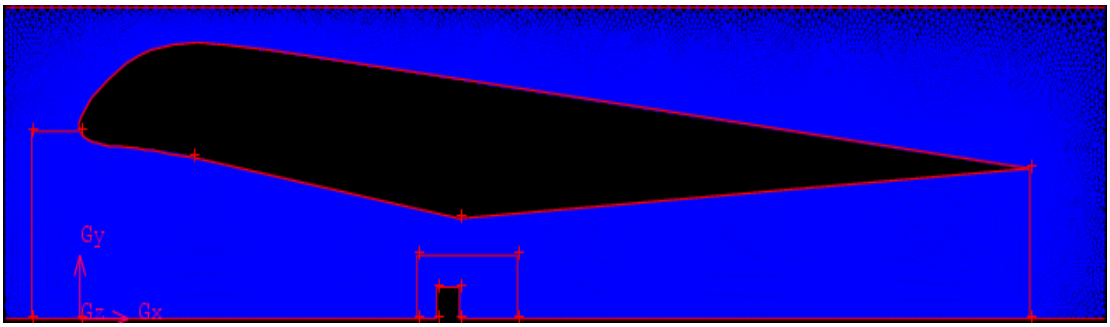

Figure 15: Zoomed image of Figure 14.

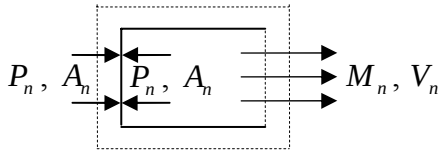

Figure 16: Free body diagram of nozzle without ejector around it.

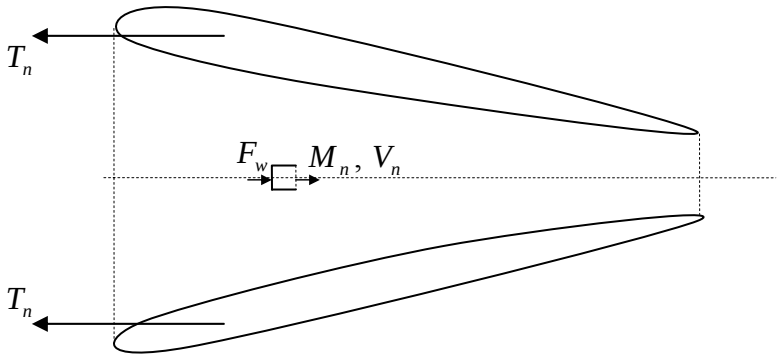

Figure 17: Free body diagram of nozzle with ejector shroud around it.

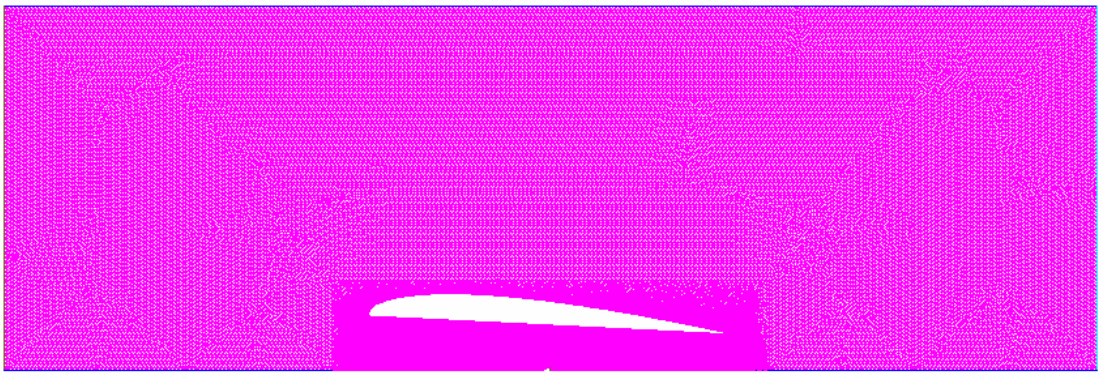

Figure 18: Jet ejector with NACA 0015 external profile meshed in GAMBIT.

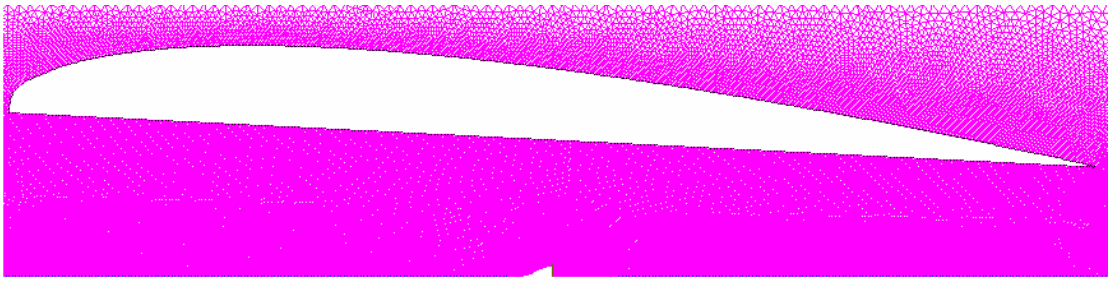

Figure 19: Zoomed image of Figure 18.

Figure 20: Axis symmetric profile of the optimized geometry.

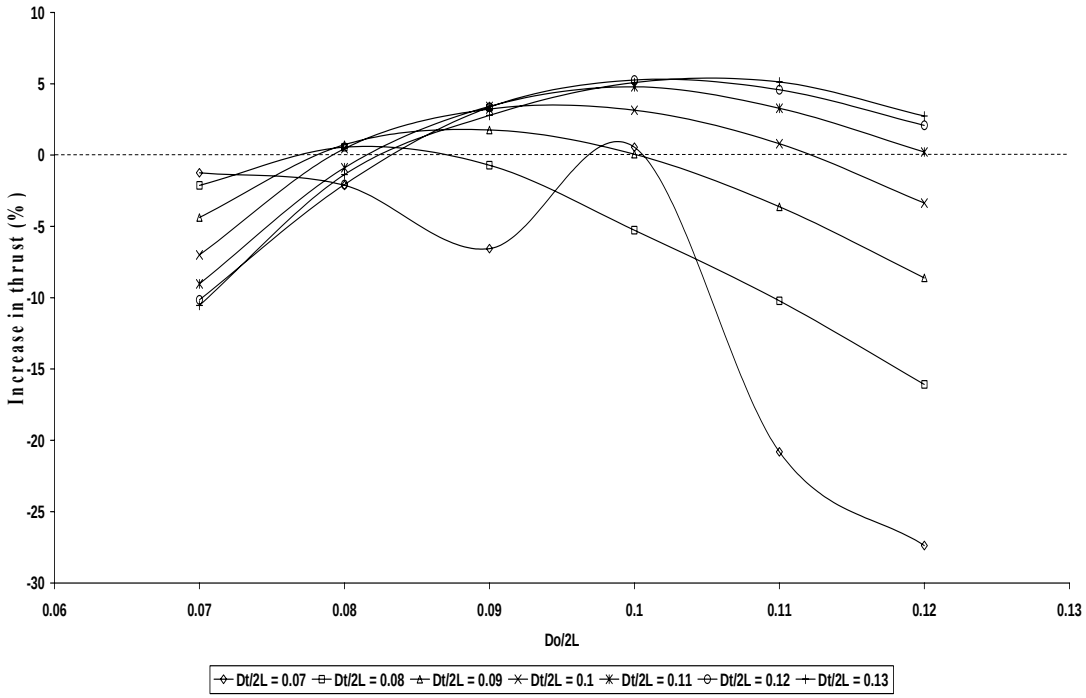

Figure 21: Percentage increase in thrust Vs $D_o/2L$ for $D_n/2L$ = 0.025, X_t/L = 0.4, $D_p/2L$ = 0.15, r = 10, V_{fs} = 6 m/s.

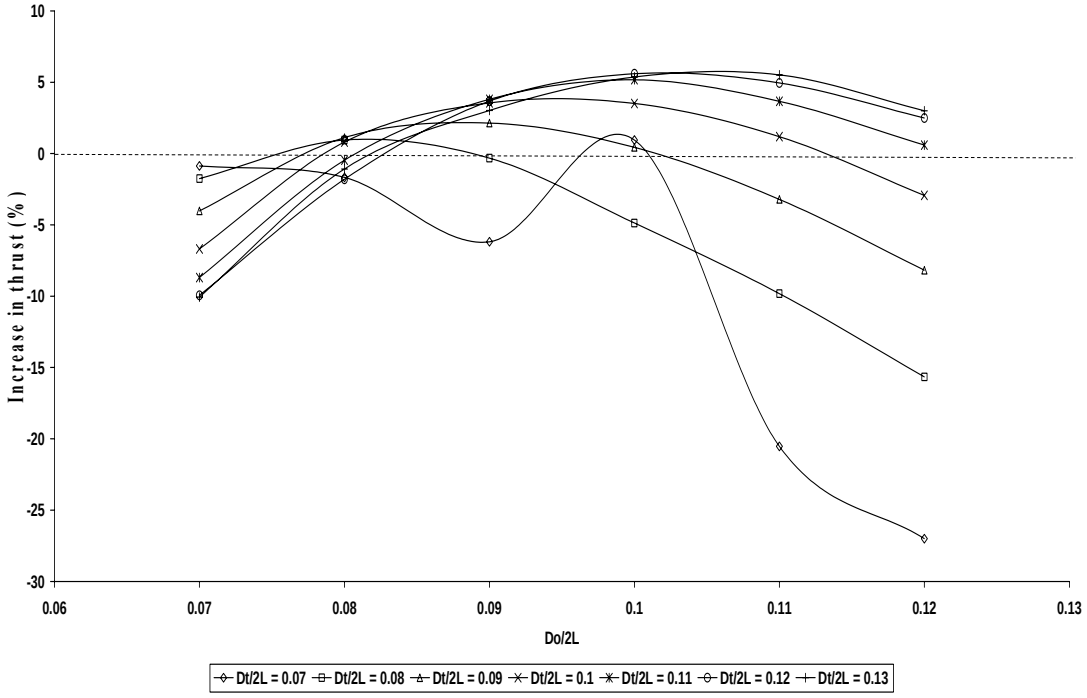

Figure 22: Percentage increase in thrust Vs $D_o/2L$ for $D_n/2L$ = 0.025, X_t/L = 0.4, $D_p/2L$ = 0.15, r = 10, V_{fs} = 10 m/s.

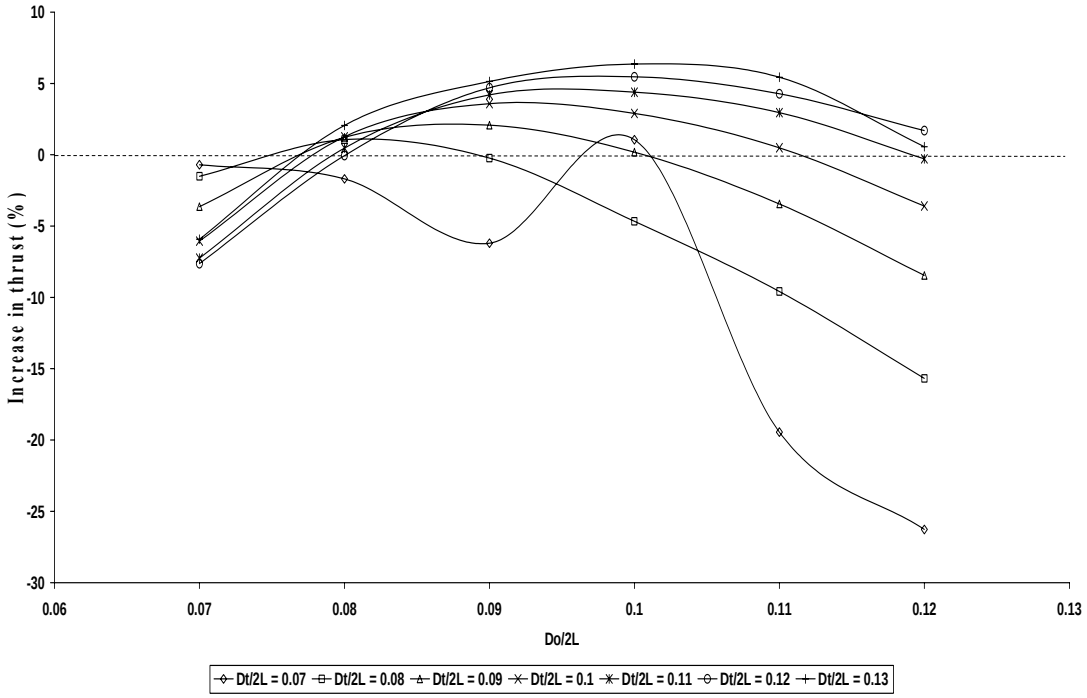

Figure 23: Percentage increase in thrust Vs $D_o/2L$ for $D_n/2L$ = 0.025, X_t/L = 0.4, $D_p/2L$ = 0.15, r = 10, V_{fs} = 15 m/s.

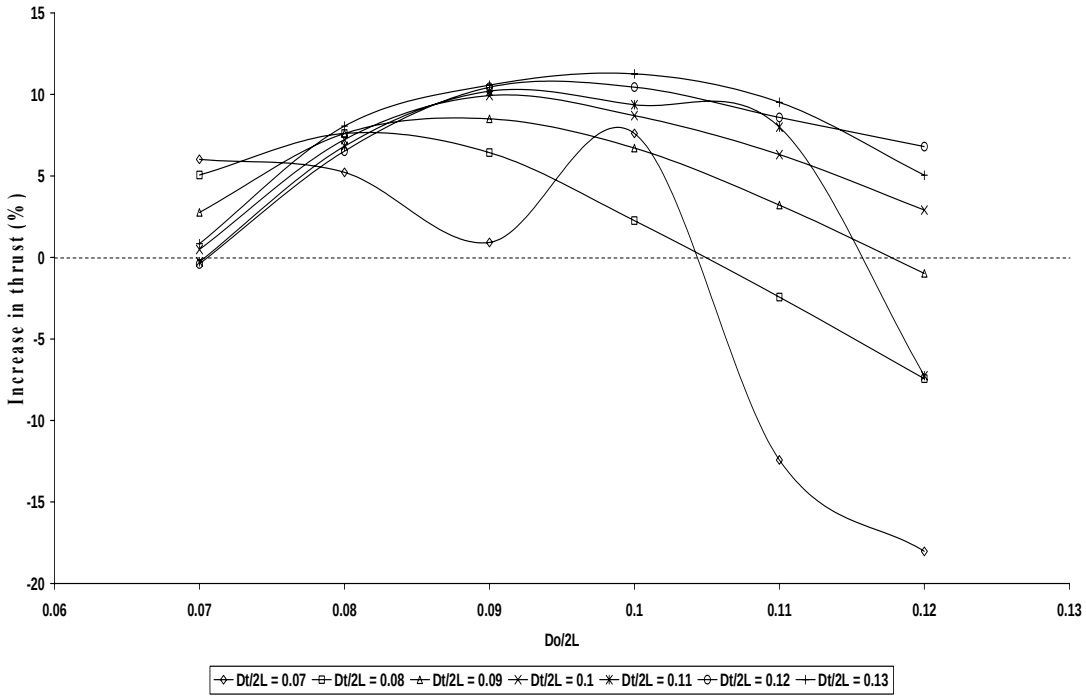

Figure 24: Percentage increase in thrust Vs $D_o/2L$ for $D_n/2L$ = 0.025, X_t/L = 0.4, $D_p/2L$ = 0.15, r = 15.

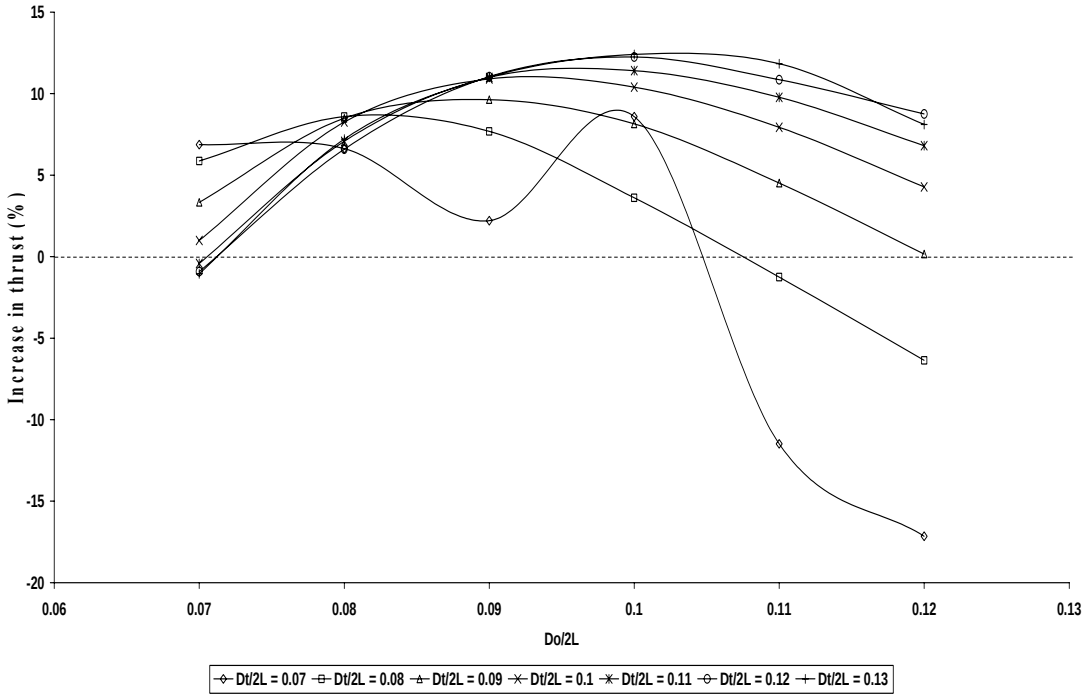

Figure 25: Percentage increase in thrust Vs $D_o/2L$ for $D_n/2L$ = 0.025, X_t/L = 0.4, $D_p/2L$ = 0.15, r = 50/3.

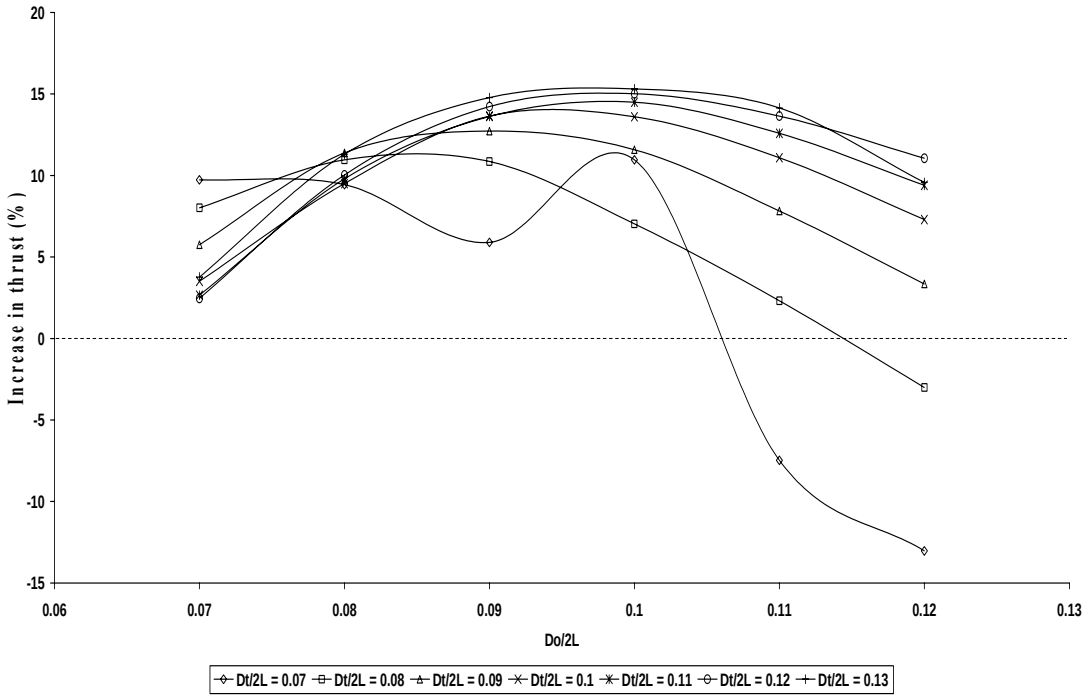

Figure 26: Percentage increase in thrust Vs $D_o/2L$ for $D_n/2L$ = 0.025, X_t/L = 0.4, $D_p/2L$ = 0.15, r = 70/3.

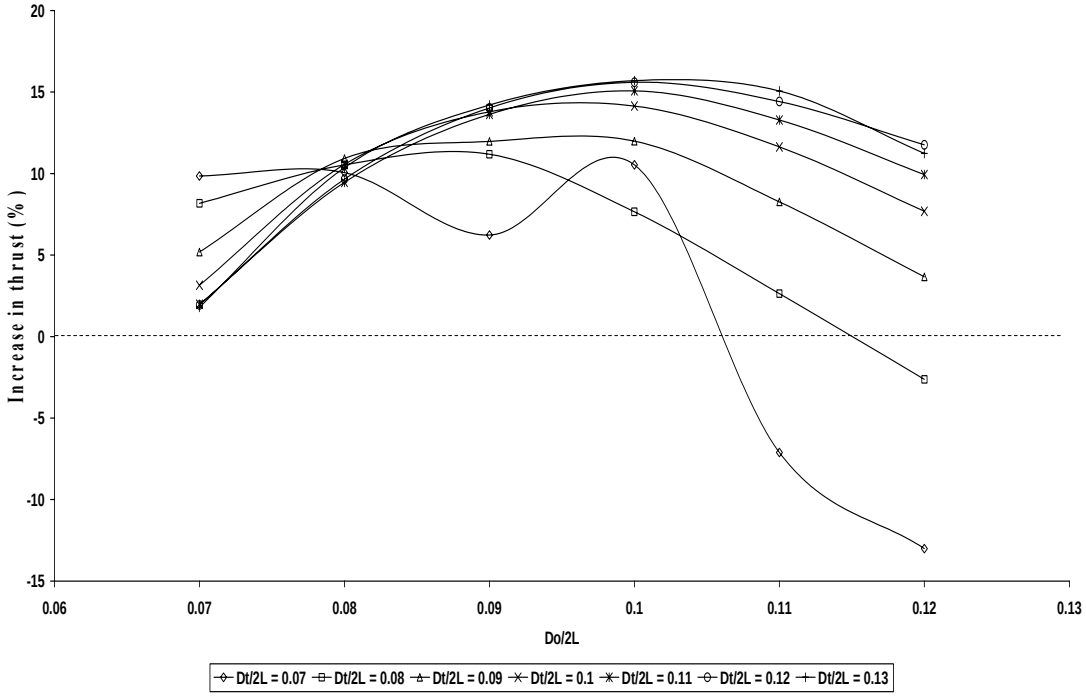

Figure 27: Percentage increase in thrust Vs $D_o/2L$ for $D_n/2L$ = 0.025, X_t/L = 0.4, $D_p/2L$ = 0.15, r = 25.

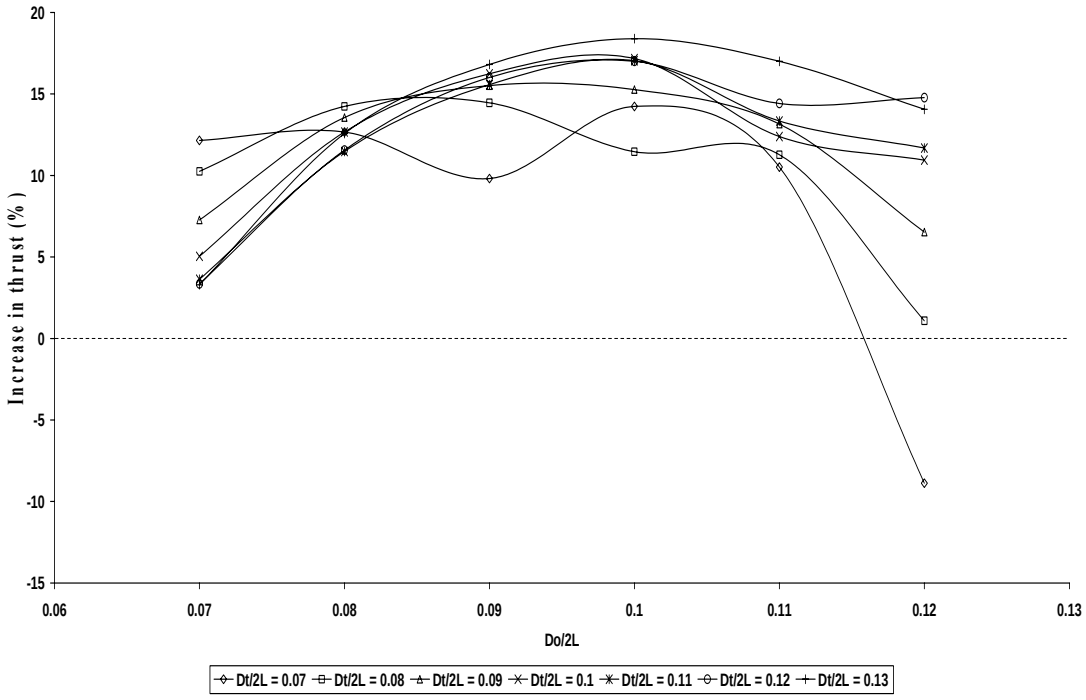

Figure 28: Percentage increase in thrust Vs $D_o/2L$ for $D_n/2L$ = 0.025, X_t/L = 0.4, $D_p/2L$ = 0.15, r = 40.

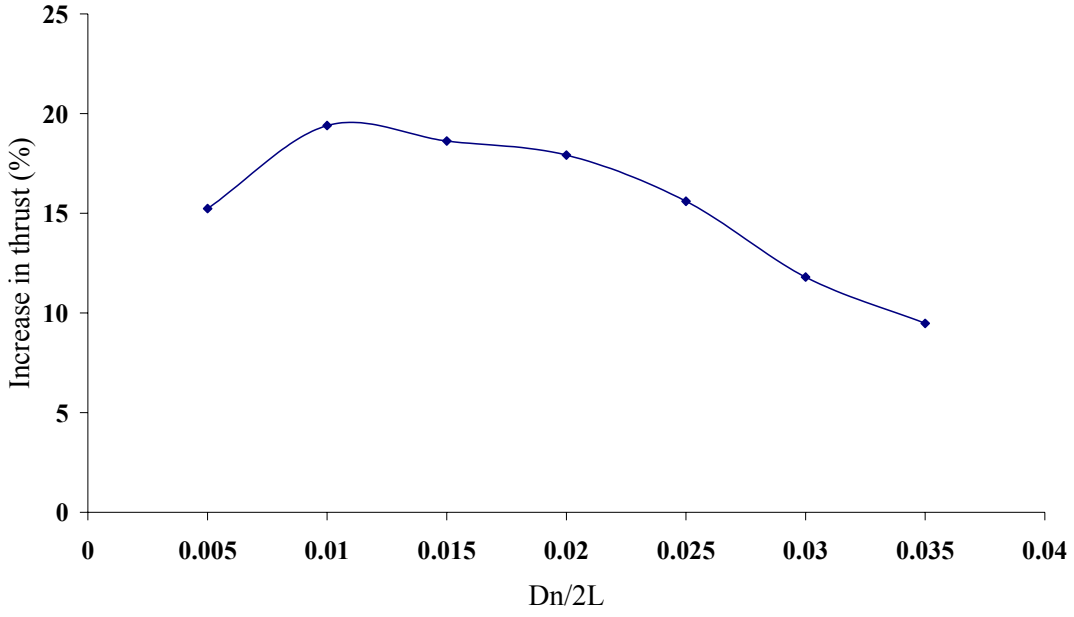

Figure 29: Percentage increase in thrust Vs D_n/2*L* for X_t/*L* = 0.4, D_p/2*L* = 0.15, D_t/2*L* = 0.12, D_o/2*L* = 0.1, V_{fs} = 2 m/s & *Re* D_n = 2.49E+06.

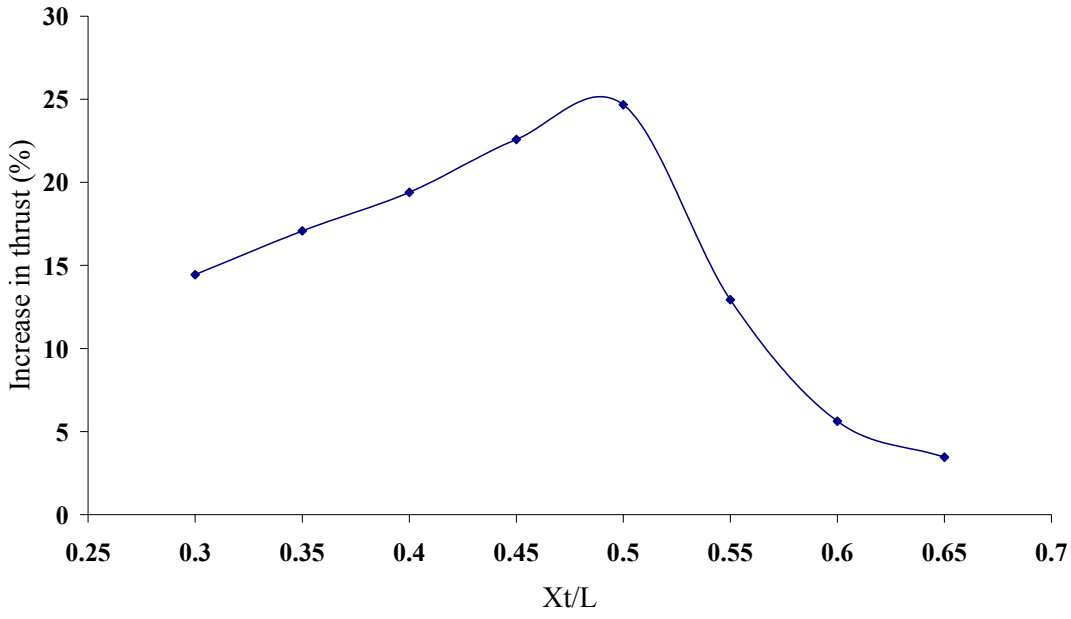

Figure 30: Percentage increase in thrust Vs X_t/L for $D_n/2L$ = 0.01, $D_p/2L$ = 0.15, $D_t/2L$ = 0.12, $D_o/2L$ = 0.1, V_{fs} = 2 m/s & *Re* D_n = 2.49E+06.

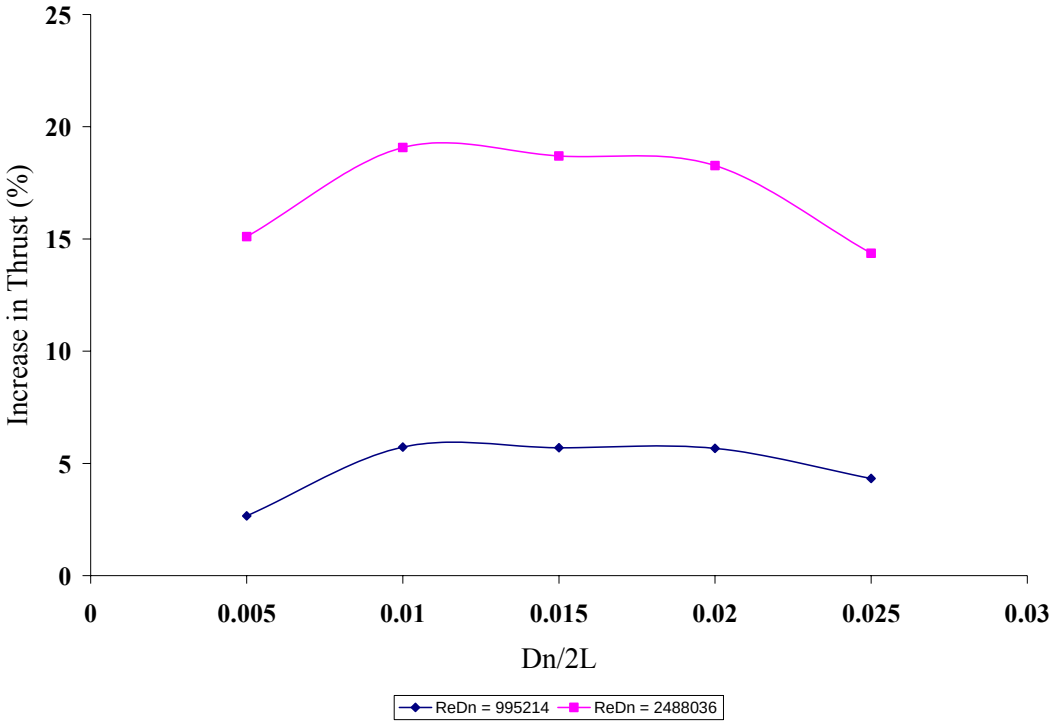

Figure 31: Percentage increase in thrust Vs $D_n/2L$ for $X_t/L = 0.4$, $D_p/2L = 0.15$, $D_t/2L = 0.125$, $D_o/2L = 0.1$ & $V_{fs} = 2$ m/s.

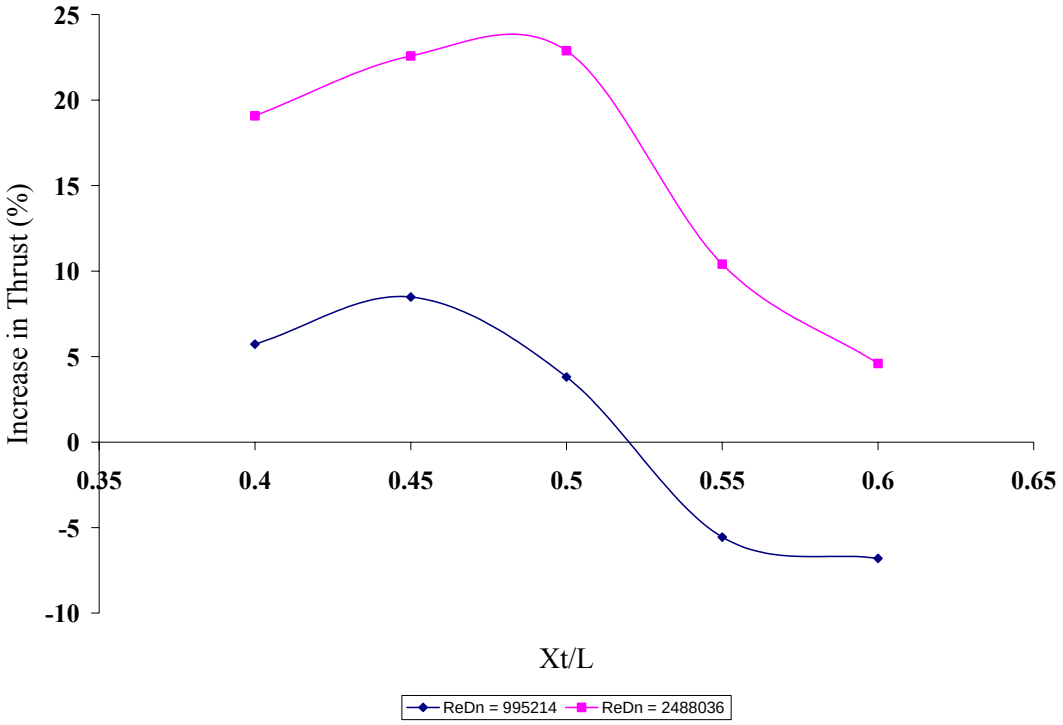

Figure 32: Percentage increase in thrust Vs X_t/L for $D_n/2L = 0.01$, $D_p/2L = 0.15$, $D_t/2L = 0.125$, $D_o/2L = 0.1$ & $V_{fs} = 2$ m/s.

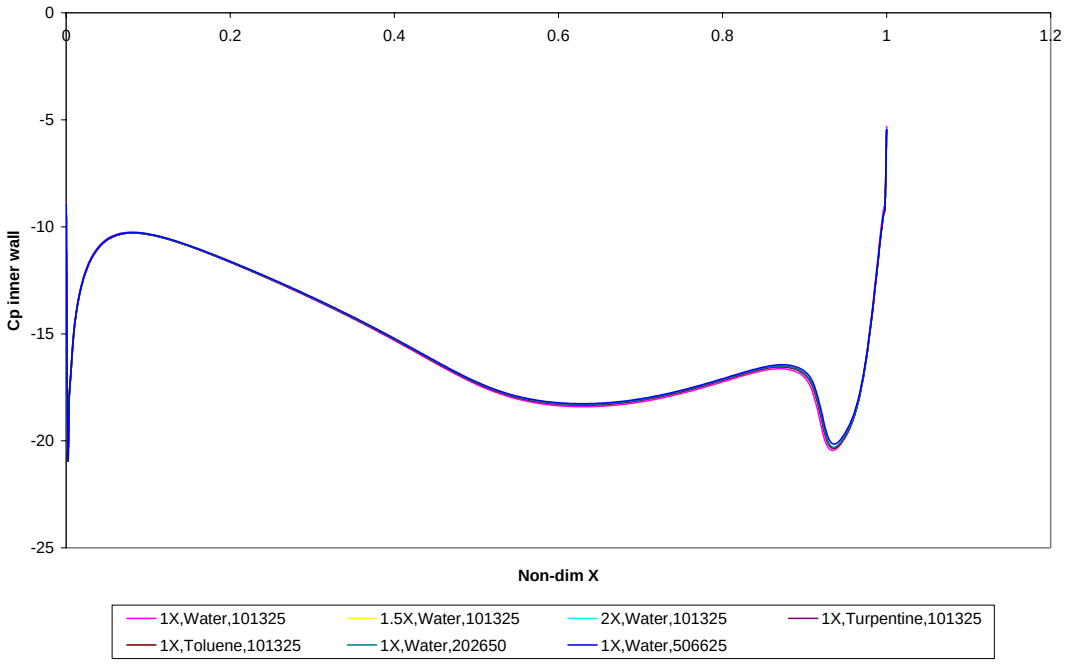

Figure 33: C_p of inner wall Vs non-dim X.

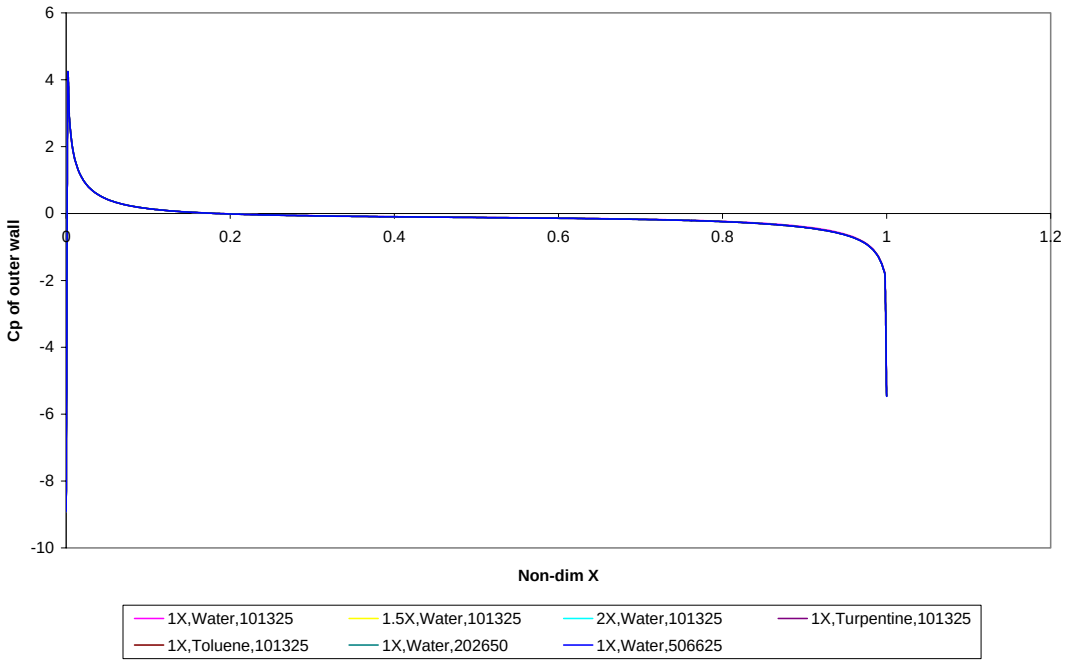

Figure 34: C_p of outer wall Vs non-dim X.

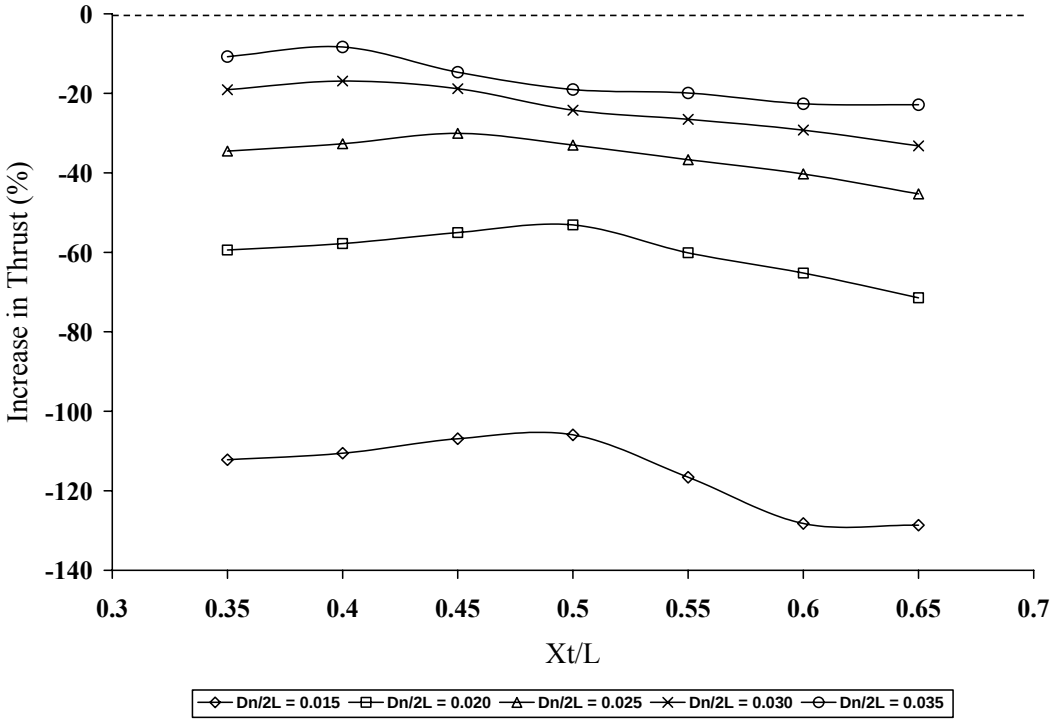

Figure 35: Percentage increase in thrust Vs X_t/L for $D_p/2L = 0.15$, $D_t/2L = 0.12$, $D_o/2L = 0.1$ & $r = 5$.

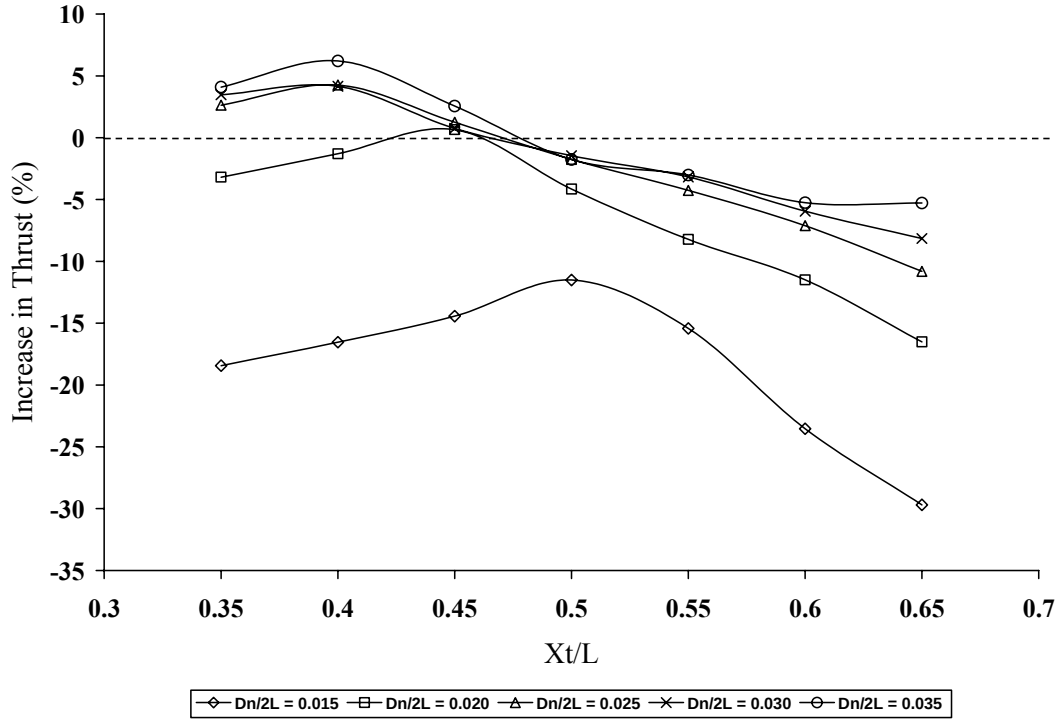

Figure 36: Percentage increase in thrust Vs X_t/L for $D_p/2L = 0.15$, $D_t/2L = 0.12$, $D_o/2L = 0.1$ & $r = 10$.

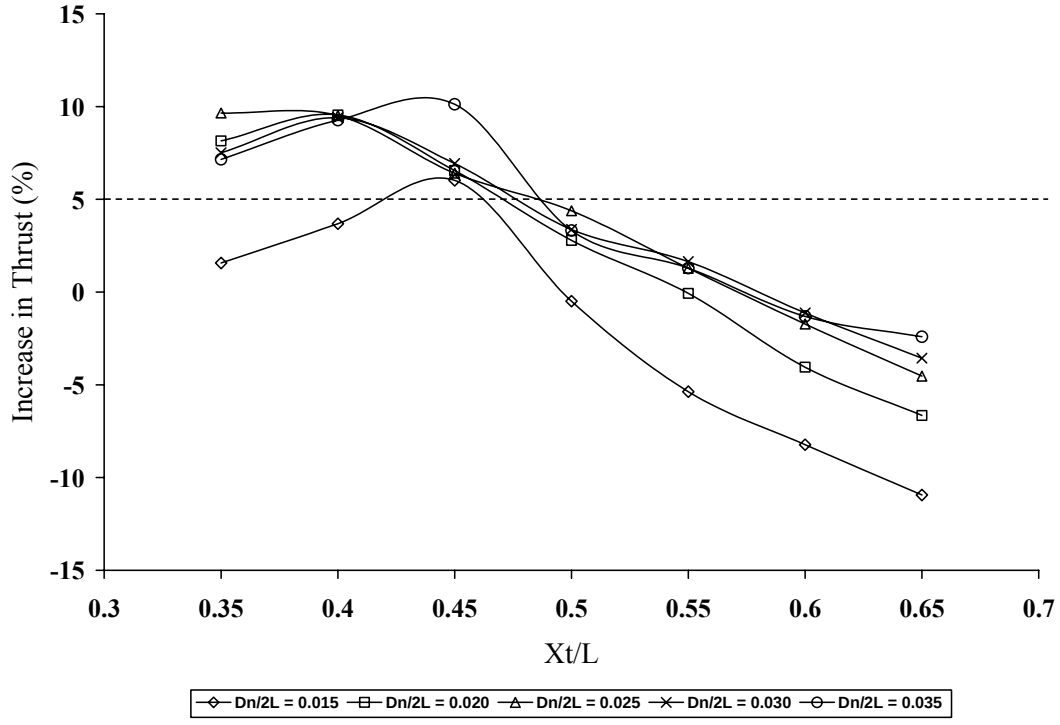

Figure 37: Percentage increase in thrust Vs X_t/L for $D_p/2L = 0.15$, $D_t/2L = 0.12$, $D_o/2L = 0.1$ & $r = 15$.

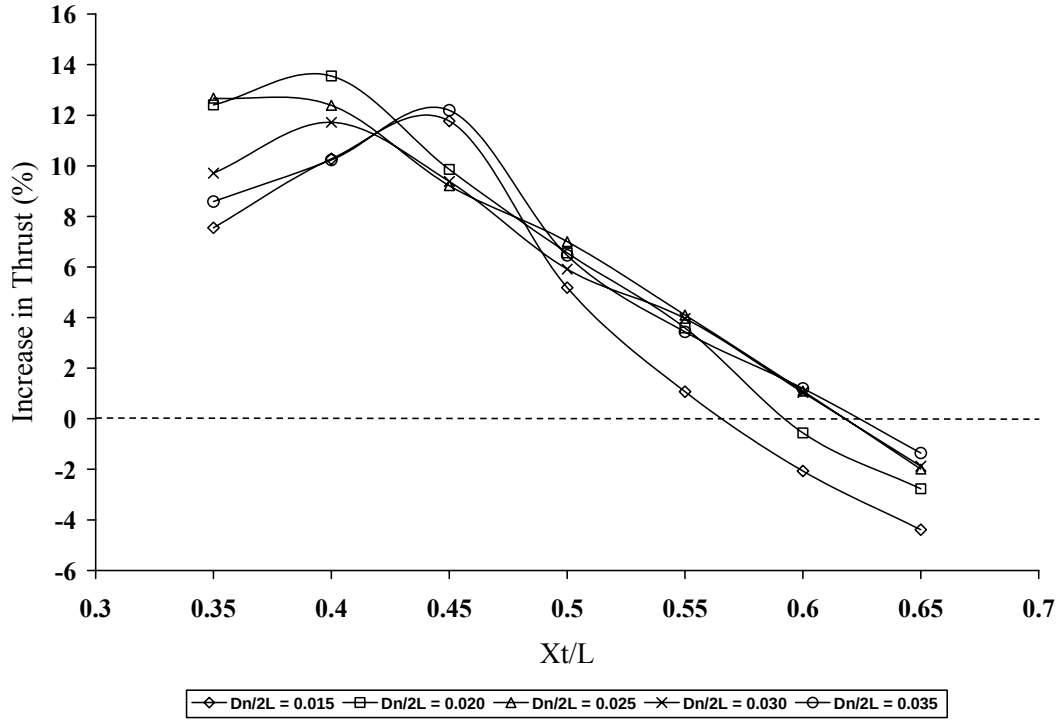

Figure 38: Percentage increase in thrust Vs $D_p/2L$ = 0.15, $D_t/2L$ = 0.12, $D_o/2L$ = 0.1 & r = 20.

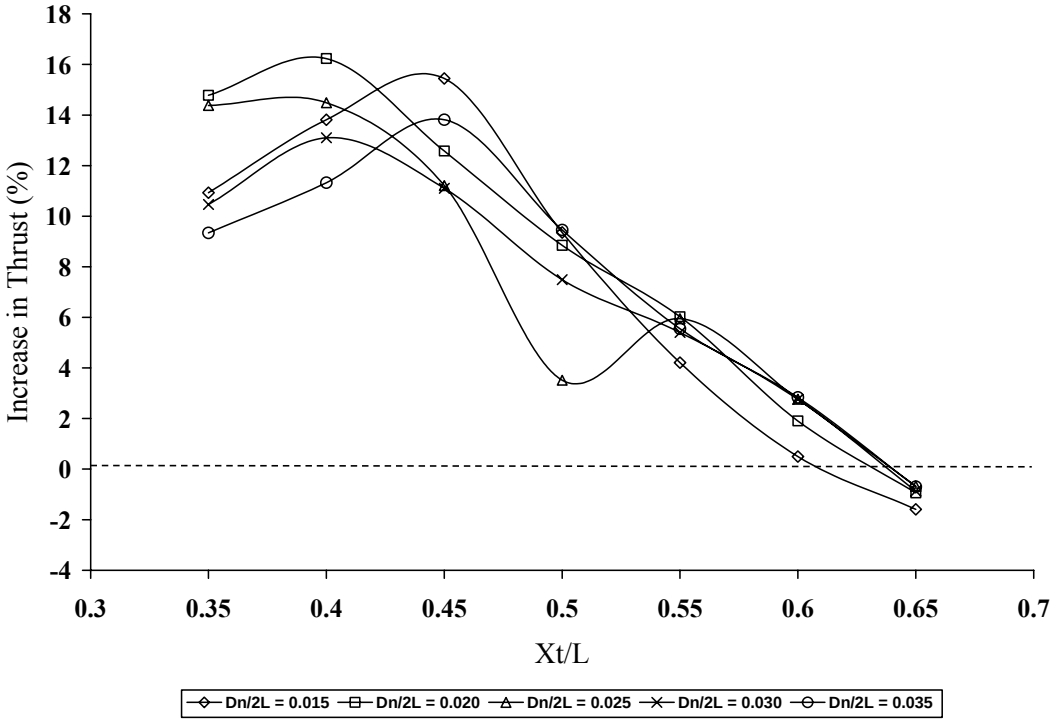

Figure 39: Percentage increase in thrust Vs X_t/L for $D_p/2L = 0.15$, $D_t/2L = 0.12$, $D_o/2L = 0.1$ & $r = 25$.

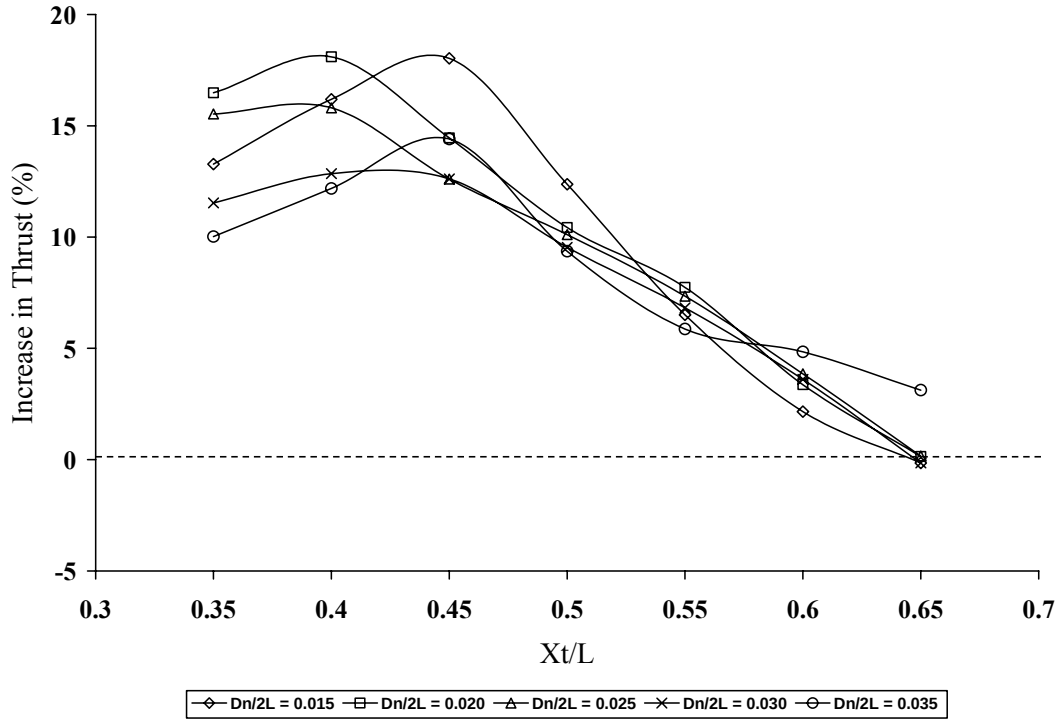

Figure 40: Percentage increase in thrust Vs X_t/L for $D_p/2L = 0.15$, $D_t/2L = 0.12$, $D_o/2L = 0.1$ & $r = 30$.

APPENDIX B

TABLES

Table 1: Same fluid and operating pressure with different scales for same Mach numbers & *GM* values.

Fluid	scale	P_{ps}	P_o	P_{ms}	M_m	M_p	GM_m	GM_p
Air	1×	101308.9	101325	101515.9	0.8513	0.01509	0.852908	0.01509
air	1.5×	101308	101325	101435.4	0.85258	0.015492	0.853512	0.01549
air	2×	101307.5	101325	101394.8	0.85253	0.015698	0.853121	0.01569

Table 2: Different Mach and *GM* values for similar conditions in Table 1.

Fluid	scale	P_{ps}	P_o	P_{ms}	M_m	M_p	GM_m	GM_p
air	1×	100974.7	101325	101612.3	1.30051	0.018911	1.304201	0.01885
air	1.5×	100973.8	101325	101601.7	1.30054	0.019272	1.304087	0.01921
air	2×	100973.4	101325	101596.8	1.30055	0.019424	1.304035	0.01936

Table 3: Different fluids with other parameters remaining same.

Fluid	scale	P_{ps}	P_o	P_{ms}	M_m	M_p	GM_m	GM_p
air	1×	101308.9	101325	101515.9	0.8513	0.01509	0.852908	0.01509
steam	1×	101308.7	101325	101529.4	0.88354	0.015732	0.885324	0.01573

Table 4: Different Mach and *GM* values for similar conditions in Table 3.

Fluid	scale	P_{ps}	P_o	P_{ms}	M_m	M_p	GM_m	GM_p
Air	1×	100974.7	101325	101612.3	1.30051	0.018911	1.304201	0.01885
steam	1×	100975	101325	101604.9	1.35039	0.019547	1.354118	0.01948

Table 5: Different operating pressures with same scale, fluid, and Mach no.

Fluid	scale	P_{ps}	P_o	P_{ms}	M_m	M_p	GM_m	GM_p
air	1×	10153.18	10132.5	10227.68	0.78842	0.013903	0.079583	0.00139
air	1×	50610.96	50662.7	50760.31	0.79338	0.013945	0.397454	0.00697
air	1×	101177.8	101325	101399.9	0.79417	0.013951	0.794761	0.01393
air	1×	505565.1	506627	506357.6	0.79503	0.01396	3.973076	0.06966
air	1×	1010933	1013253	1012449	0.79522	0.013963	7.945888	0.13931

Table 6: Different Mach no. and operating pressures with same scale and fluid.

Fluid	scale	P_{ps}	P_o	P_{ms}	M_m	M_p	GM_m	GM_p
air	1×	10092.42	10132.6	10176.92	1.55087	0.022446	0.155767	0.00224
air	1×	50654.8	50662.5	50700.01	0.3089	0.004473	0.154566	0.00224
air	1×	101321.1	101325	101343.8	0.15562	0.002236	0.155647	0.00224

Table 7: Different Mach no., *GM* values and operating pressures with same scale and fluid.

Fluid	scale	P_{ps}	P_o	P_{ms}	M_m	M_p	GM_m	GM_p
air	1×	506486.5	506625	506537.2	0.33372	0.005992	1.66829	0.02995
air	1×	1013179	1013250	101320.6	0.1682	0.002995	1.681967	0.02995

Table 8: Different scale, fluid, operating pressure and Mach no. for $GM_m \approx 0.22$ and $GM_p \approx 0.0032$.

Fluid	scale	P_{ps}	P_o	P_{ms}	M_m	M_p	GM_m	GM_p	Symbol on Figure 11
air	1×	25285.24	25331.3	25503.06	0.87127	0.012617	0.219294	0.00315	1
Steam	1.5×	75975.15	75993.8	76020.73	0.30384	0.004349	0.227962	0.00326	2
N_2	2×	227974.2	227981	227988.3	0.09729	0.001401	0.218904	0.00315	3

Table 9: Different scale, fluid, operating pressure and Mach no. for $GM_m \approx 1.2$ and $GM_p \approx 0.02$.

Fluid	scale	P_{ps}	P_o	P_{ms}	M_m	M_p	GM_m	GM_p	Symbol on Figure 12
N_2	1×	1013208	1013250	1013248	0.11989	0.001983	1.198887	0.01983	a
air	1.5×	506535.2	506625	506607.4	0.24002	0.003982	1.200062	0.01991	b
steam	2×	100823.4	101326	101554.4	1.24368	0.020786	1.246498	0.02068	c

Table 10: Optimized dimensionless quantities in first iteration.

$D_n/2L$	X_t/L	$D_p/2L$	$D_t/2L$	$D_o/2L$
0.01	0.5	0.15	0.125	0.1

Table 11: Comparison of percentage increase in thrust for various external profiles.

Profile	**Increase in thrust (%)**
Standard	22.888
Flat	23.429
NACA 0012	20.697
NACA 0015	20.152
NACA 0018	19.753
NACA 0021	19.282

Table 12: Percentage increase in thrust for velocity ratio of *r* = 15, $D_p/2L$ = 0.1 and 0.2

$D_n/2L$	X_t/L	$D_p/2L$	$D_t/2L$	$D_o/2L$	**Increase in thrust (%)**
0.01	0.3	0.1	0.07	0.07	-4.0765
0.01	0.4	0.1	0.07	0.07	-2.3826
0.01	0.5	0.1	0.07	0.07	-2.4802
0.02	0.3	0.1	0.07	0.07	4.4273
0.02	0.4	0.1	0.07	0.07	5.6878
0.02	**0.5**	**0.1**	**0.07**	**0.07**	**6.2502**
0.02	0.6	0.1	0.07	0.07	0.2129
0.03	0.3	0.1	0.07	0.07	1.7684
0.03	0.4	0.1	0.07	0.07	2.3435
0.03	0.5	0.1	0.07	0.07	3.4878
0.03	0.6	0.1	0.07	0.07	-0.055
0.01	0.3	0.2	0.15	0.12	-31.322
0.01	0.4	0.2	0.15	0.12	-43.008
0.01	0.5	0.2	0.15	0.12	-43.36
0.02	0.2	0.2	0.15	0.12	3.83
0.02	0.3	0.2	0.15	0.12	6.6776
0.02	0.4	0.2	0.15	0.12	-2.7096
0.02	0.5	0.2	0.15	0.12	-10.749
0.03	0.1	0.2	0.15	0.12	4.2681
0.03	**0.2**	**0.2**	**0.15**	**0.12**	**9.2637**
0.03	0.3	0.2	0.15	0.12	7.7352
0.03	0.4	0.2	0.15	0.12	4.2842
0.03	0.5	0.2	0.15	0.12	-2.7748

Table 13: Percentage increase in thrust for velocity ratio of *r* = 15 and $D_p/2L$ = 0.15

$D_n/2L$	X_t/L	$D_p/2L$	$D_t/2L$	$D_o/2L$	**Increase in thrust (%)**
0.035	0.45	0.15	0.12	0.1	10.126

Table 14: Combinations of scale, fluid and ambient pressure used for analysis.

No	**Scale**	**Fluid**	P_∞ **(atm)**	ρ **(kg/m^3)**	μ **(kg/ms)**
1	1×	Water	101325	998.2	0.001
2	1.5×	Water	101325	998.2	0.001
3	2×	Water	101325	998.2	0.001
4	1×	Turpentine	101325	855	0.0015
5	1×	Toluene	101325	866	0.0006
6	1×	Water	202650	998.2	0.001
7	1×	Water	506625	998.2	0.001

Table 15: Comparison of percentage increase in thrust for these combinations.

No	T (N)	T^1 (N)	Increase in thrust (%)
1	6046	4899	23.43
2	6041	4899	23.33
3	6041	4899	23.32
4	15504	12570	23.34
5	2377	1927	23.34
6	6041	4899	23.32
7	6038	4899	23.25

APPENDIX C

JOURNAL FILE

solver select "FLUENT 5/6"

/ y = 0.5* D_p ---------- 1

vertex create coordinates 0 100 0

/ x = 0.3* X_t and y = 0.35* D_p +0.15* D_t ---------- 2

vertex create coordinates 240 85 0

/ y = 0.5* D_o ---------- 3

vertex create coordinates 1000 70 0

/ x = 0.15* X_t and y = 0.4* D_p +0.1* D_t ---------- 4

vertex create coordinates 120 90 0

/ x = X_t -0.5* D_n ---------- 5

vertex create coordinates 796 0 0

/ x = X_t -0.5* D_n and y = 0.5* D_n ---------- 6

vertex create coordinates 796 4 0

/ x = X_t and y = 0.5* D_n ---------- 7

vertex create coordinates 800 4 0

/ x = X_t ---------- 8

vertex create coordinates 800 0 0

vertex create coordinates -1000 0 0

vertex create coordinates -1000 1000 0

vertex create coordinates 2000 1000 0

vertex create coordinates 2000 0 0

vertex create coordinates 0 0 0

vertex create coordinates 1000 0 0

/ x = X_t -45 and y = D_n ---------- 9

vertex create coordinates 755 8 0

/ x = X_t +60 and y = D_n ---------- 10

vertex create coordinates 860 8 0

/ x = X_t +60 ---------- 11

vertex create coordinates 860 0 0

/ x = X_t -45 ---------- 12

vertex create coordinates 755 0 0

vertex create coordinates 1500 0 0

vertex create coordinates -500 0 0

vertex create coordinates -500 500 0

vertex create coordinates 1500 500 0

vertex create coordinates -100 0 0

vertex create coordinates 1100 0 0

vertex create coordinates 1100 250 0

vertex create coordinates -100 250 0

/ x = X_t and y = 0.5* D_t ---------- 13

vertex create coordinates 800 50 0

/ x = 50 and y = D_p + 55 ---------- 14

vertex create coordinates 50 155 0

/ x = 100 and y = D_p + 70 ---------- 15

vertex create coordinates 100 170 0

/ x = 200 and y = D_p + 65 ---------- 16

vertex create coordinates 200 165 0

edge create straight "vertex.10" "vertex.9"

edge create straight "vertex.9" "vertex.5"

edge create straight "vertex.5" "vertex.6"

edge create straight "vertex.6" "vertex.7"

```
edge create straight "vertex.7" "vertex.8"

edge create straight "vertex.8" "vertex.12"

edge create straight "vertex.12" "vertex.11"

edge create straight "vertex.10" "vertex.11"

edge create nurbs "vertex.2" "vertex.4" "vertex.1" "vertex.28" "vertex.29" \

  "vertex.30" "vertex.3" interpolate

edge create straight "vertex.2" "vertex.27"

edge create straight "vertex.27" "vertex.3"

edge split "edge.9" vertex "vertex.1" connected

vertex delete "vertex.4" "vertex.28" "vertex.29" "vertex.30"

edge split "edge.2" vertex "vertex.13" connected

edge split "edge.6" vertex "vertex.14" connected

edge create straight "vertex.1" "vertex.13"

edge create straight "vertex.3" "vertex.14"

edge split "edge.13" vertex "vertex.18" connected

edge split "edge.6" vertex "vertex.17" connected

edge create straight "vertex.18" "vertex.15"

edge create straight "vertex.15" "vertex.16"
```

edge create straight "vertex.16" "vertex.17"

edge split "edge.2" vertex "vertex.20" connected

edge split "edge.14" vertex "vertex.19" connected

edge create straight "vertex.20" "vertex.21"

edge create straight "vertex.21" "vertex.22"

edge create straight "vertex.22" "vertex.19"

edge split "edge.22" vertex "vertex.23" connected

edge split "edge.14" vertex "vertex.24" connected

edge create straight "vertex.23" "vertex.26"

edge create straight "vertex.26" "vertex.25"

edge create straight "vertex.25" "vertex.24"

/ y = 0.5* D_p ---------- 17

vertex create coordinates -50 100 0

vertex create coordinates -50 0 0

edge create straight "vertex.1" "vertex.28"

edge create straight "vertex.28" "vertex.29"

edge split "edge.27" vertex "vertex.29" connected

edge delete "edge.15" lowertopology

```
physics create "Domain Inlet" btype "VELOCITY_INLET" edge "edge.1"

physics create "Domain Outlet" btype "OUTFLOW" edge "edge.7"

physics create "Jet Inlet" btype "INTERIOR" edge "edge.33" "edge.32"

physics create "Jet outlet" btype "INTERIOR" edge "edge.16"

physics create "Nozzle" btype "VELOCITY_INLET" edge "edge.5"

physics create "Axis" btype "AXIS" edge "edge.2" "edge.13" "edge.6" "edge.14" \
  "edge.17" "edge.18" "edge.22" "edge.27" "edge.28" "edge.23" "edge.34"

physics create "Jet outer surface" btype "WALL" edge "edge.12"

physics create "Jet inner surface" btype "WALL" edge "edge.9" "edge.10" \
  "edge.11"

physics create "Nozzle wall" btype "WALL" edge "edge.3" "edge.4"

physics create "Domain Boundary" btype "SYMMETRY" edge "edge.8"

face create "Jet Core" wireframe "edge.17" "edge.3" "edge.4" "edge.5" \
  "edge.6" "edge.21" "edge.20" "edge.19" real

face create "Jet inner" wireframe "edge.13" "edge.34" "edge.33" "edge.32" \
  "edge.9" "edge.10" "edge.11" "edge.16" "edge.18" "edge.21" "edge.20" \
  "edge.19" real

face create "Jet outer 0" wireframe "edge.32" "edge.33" "edge.27" "edge.29" \
```

```
  "edge.30" "edge.31" "edge.14" "edge.16" "edge.12" real
face create "Jet outer 1" wireframe "edge.29" "edge.22" "edge.24" "edge.25" \
  "edge.26" "edge.28" "edge.30" "edge.31" real
face create "Jet outer 2" wireframe "edge.24" "edge.2" "edge.1" "edge.8" \
  "edge.7" "edge.23" "edge.26" "edge.25" real
physics create "Fluid Medium" ctype "FLUID" face "Jet Core" "Jet outer 1" \
  "Jet outer 2" "Jet outer 0" "Jet inner"
undo begingroup
edge picklink "edge.3"
edge mesh "edge.3" successive ratio1 1 intervals 24
undo endgroup
undo begingroup
edge picklink "edge.4"
edge mesh "edge.4" successive ratio1 1 intervals 24
undo endgroup
undo begingroup
edge picklink "edge.5"
edge mesh "edge.5" successive ratio1 1 intervals 24
```

```
undo endgroup

undo begingroup

edge modify "edge.17" backward

edge picklink "edge.17"

edge mesh "edge.17" successive ratio1 1.02 size 0.5

undo endgroup

undo begingroup

edge picklink "edge.6"

edge mesh "edge.6" successive ratio1 1.015 size 0.55

undo endgroup

face mesh "Jet Core" triangle size 1

face mesh "Jet inner" triangle size 1.5

undo begingroup

edge picklink "edge.12"

edge mesh "edge.12" successive ratio1 1 size 1.5

undo endgroup

undo begingroup

edge picklink "edge.14"
```

```
edge mesh "edge.14" successive ratio1 1.04 size 5

undo endgroup

undo begingroup

edge modify "edge.27" backward

edge picklink "edge.27"

edge mesh "edge.27" successive ratio1 1.04 size 5

undo endgroup

face mesh "Jet outer 0" triangle size 10

face mesh "Jet outer 1" triangle size 10

face mesh "Jet outer 2" triangle size 10

export Fluent5 "xb6.msh" nozval
```

VITA

Name: Ganesh Mohan

Email: ganesh.mohan@atkinsamericas.com

Address: 2700 Woodland Park Dr., Apt 515
Houston, Texas 77082

Education:

M.S., Mechanical Engineering (May 2006)
Texas A&M University
(http://www.tamu.edu)
College Station, Texas 77843-3123

B.Tech, Mechanical Engineering (Aug 2003)
Indian Institute of Technology Madras
(http://www.iitm.ac.in)
Chennai, India

Work Experience:

02/06-Present — Consultant, Safety Group
WS Atkins Inc.
(http://www.atkinsglobal.com)
2925 Briarpark Drive, Suite 550
Houston, Texas 77042

01/04-01/06 — Graduate Research Assistant
Fluid Dynamics Laboratory
Aerospace Engineering Department
(http://aero.tamu.edu)
Texas A&M University
College Station, Texas 77843-3123

09/03-12/03 — Teaching Assistant
Heat Transfer (MEEN-461)
Mechanical Engineering Department
(http://www.mengr.tamu.edu)
Texas A&M University
College Station, Texas 77843-3123

PEER REVIEWED PUBLICATION

Mohan, G., Rao, B. P., Das, S. K., Pandiyan, S., Rajalakshmi, N., et al., 2004, "Analysis of Flow Maldistribution of Fuel and Oxidant in a PEMFC," ASME Journal of Energy Resources Technology, **126**, pp. 262-270.